

# International PhD School "F. Lucchin": Science and Technology with E-ELT

## Indirect Imaging of Ultra-Cool Dwarfs

Erice, Italie

10h00-11h00, Saturday October 10<sup>th</sup> 2015

France Allard

Directrice de Recherche (DR2), CNRS  
Centre de Recherche Astrophysique de Lyon  
Site ENS-Lyon





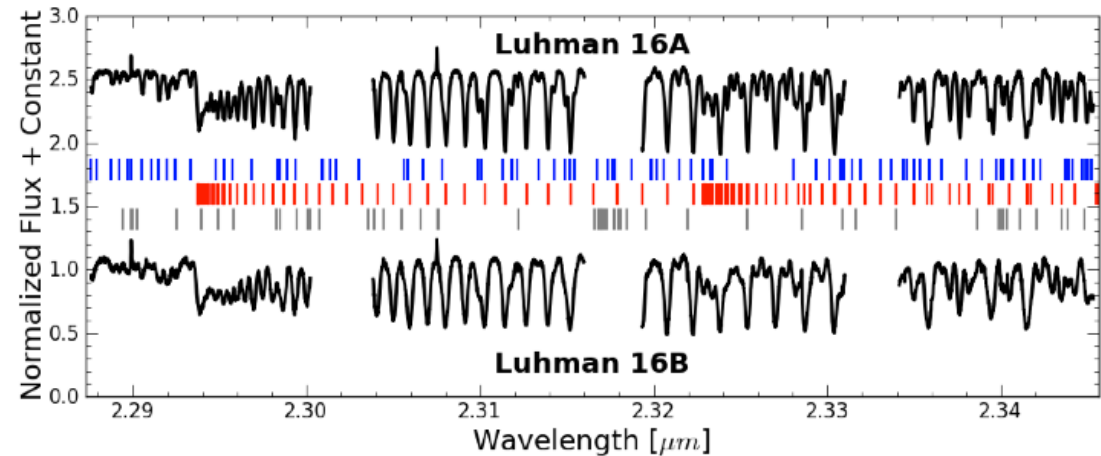
# Surface inhomogeneities revealed by Doppler imaging !

*Crossfield et al. (Nature 505, 2014)*

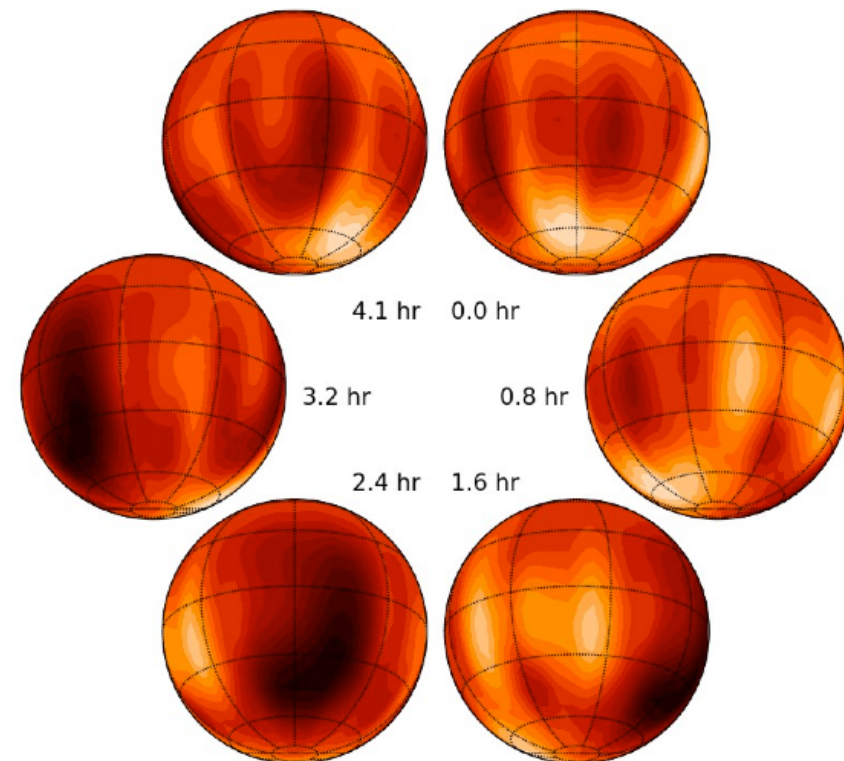
**L7.5 + T0.5 @ 2 pc**

High-resolution, near-infrared spectra of the Luhman 16AB brown dwarfs (black curves). The vertical ticks indicate absorption features: H<sub>2</sub>O (blue) and CO (red), and residual telluric features (gray). The lines of the B component are broader.

Surface map of brown dwarf Luhman 16B, which clearly depicts a bright near-polar region (seen in the upper-right panels) and a darker mid-latitude area (lower-left panels) consistent with large-scale cloud inhomogeneities. The lightest and darkest regions shown correspond to brightness variations of roughly  $\pm 10\%$ . The time index of each projection is indicated near the center of the figure.



CO imaging



# Outline of this Lecture

## Introduction to the problem of UCDs surface imaging

- The PHOENIX BT-Settl models as an example of 1D classic approach
  - The 1D model assumptions and limitations
  - M, L, T and Y dwarf results
  - The cloud model used and its upgrade possibilities
  - The CO5BOLD group and code description, exp. of principal results
  - Local 3D simulations of M-L dwarfs and their implications for the validity of the 1D approach
- Surface properties of Ultra Cool Dwarfs
  - History
  - Observed Variability of L3-T8 dwarfs, their rotation properties
  - Indirect Imaging Results for the  $T_{\text{eff}} \approx 1400\text{K}$  T dwarf Luhman 16B
- Outline of Next Lecture

# Navier-Stokes Equation

intern + kinetic

$$e = u + \frac{1}{2} \vec{v} \cdot \vec{v} = u + \frac{1}{2} v^2$$

In fluid mechanics, the Navier-Stokes equations are non-linear partial derivative equations that describe fluid movements in the approximation of continuous media. These model for instance the air movements in the atmosphere, the oceanic currents, the flow of liquid water in a tube, and various other fluid flow phenomena. They are named after two XIXe century physicists, Claude Navier et George Stokes. For a not very dense gas, it is possible to derive these equations from the Boltzmann equation. Solving analytically the Navier-Stokes equations constitute one of the problems of *the price of the millennium*.

Forms of the Navier-Stokes equations are expressed in different forms. These forms depend on the notations used. Hence, several equivalent expressions of the differential operators exist.

The differential formulation of the equations in cartesian coordinates (Euler equations) and SI units is :

\* Continuity equation (or mass conservation equation) :

$$\frac{\partial \rho}{\partial t} + \text{div}(\rho \vec{v}) = 0$$

Sum of spatial derivatives

Mass flux through the surfaces of the cells. Conservation depends on boundary conditions, closed or open.

\* Quantity of movement conservation equation :

$$\frac{\partial (\rho \vec{v})}{\partial t} + \text{div}(\rho \vec{v} \otimes \vec{v}) = -\overrightarrow{\text{grad}}(p) + \text{div}(\vec{\tau}) + \rho \vec{f}$$

Diadic product gives a matrix

Work exerted by pressure

\* Energy conservation equation :

$$\frac{\partial (\rho e)}{\partial t} + \text{div}[(\rho e + p) \vec{v}] = \text{div}(\vec{\tau} \cdot \vec{v}) + \rho \vec{f} \cdot \vec{v} - \text{div}(\vec{q}) + r$$

Energy advection term

Scalar product of work exerted by gravity

Where  $\vec{f}$  designates the balance of the mass forces exerting on the fluid ( $\text{N kg}^{-1}$ ) ;  $e$  is the total energy per mass unit ( $\text{J kg}^{-1}$ ) ;  $\vec{q}$  is the heat lost by thermal conduction ( $\text{J m}^{-2} \text{s}^{-1}$ ) ;  $r$  is the loss of specific heat due to radiation ( $\text{J m}^{-3} \text{s}^{-1}$ ) ;  $\vec{\tau}$  the viscosity tensor.



# Navier-Stokes Equation

intern + kinetic

$$e = u + \frac{1}{2} \vec{v} \cdot \vec{v} = u + \frac{1}{2} v^2$$

In fluid mechanics, the Navier-Stokes equations are non-linear partial derivative equations that describe fluid movements in the atmosphere, the ocean, and various other fluid flow phenomena. They are named after George Stokes. For a not very dense gas, it is possible to solve the Navier-Stokes equations analytically. Solving analytically is a challenge that has persisted for over a millennium.

Forms of the Navier-Stokes equations depend on the notations used. Hence, several different forms exist.

The differential formulation (in vector equations) and SI units is :

\* Continuity equation (or mass conservation equation) :

Diadic product  
gives a matrix

$$\frac{\partial \rho}{\partial t} + \text{div}(\rho \vec{v}) = 0$$

Mass flux through the  
surfaces of the cells.  
Conservation depends on  
boundary conditions,  
closed or open.

\* Quantity of movement conservation equation :

Work exerted by pressure

$$\frac{\partial (\rho \vec{v})}{\partial t} + \text{div}(\rho \vec{v} \otimes \vec{v}) = -\text{grad}(p) + \text{div}(\vec{\tau}) + \rho \vec{f}$$

\* Energy conservation equation :

$$\frac{\partial (\rho e)}{\partial t} + \text{div}[(\rho e + p) \vec{v}] = \text{div}(\vec{\tau} \cdot \vec{v}) + \rho \vec{f} \cdot \vec{v} - \text{div}(\vec{q}) + r$$

Energy advection term

Scalar product of work exerted by gravity

Where  $\vec{f}$  designates the balance of the mass forces exerting on the fluid ( $\text{N kg}^{-1}$ ) ;  $e$  is the total energy per mass unit ( $\text{J kg}^{-1}$ ) ;  $\vec{q}$  is the heat lost by thermal conduction ( $\text{J m}^{-2} \text{s}^{-1}$ ) ;  $r$  is the loss of specific heat due to radiation ( $\text{J m}^{-3} \text{s}^{-1}$ ) ;  $\vec{\tau}$  the viscosity tensor.

# Classical 1D Model Construction

RHD simulations, especially in 2D and 3D, are computationally expensive, and, when treating - if at all - radiative transfer, can currently be performed only for a restricted number of wavelengths, or wavelength bins (typically 4 to 12). The classical 1D approximation simplifies the problem for a benefice on the spectral coverage and complexity level (time-dependent RT, NLTE, scattering, elemental diffusion, cloud modeling, Zeeman splitting, polarimetry, etc.) solved from the first principles, and systematically neglects:

- **Detailed Hydrodynamic Motions:** Neglecting motions in modeling the photospheres of late type M dwarf stars, brown dwarfs, and planets is acceptable since the convection, unlike in solar type stars, is efficient and the related gas velocities are small, and since wide absorption lines due to collisional broadening prevails in these atmospheres. But motions are not negligible in the case of the disequilibrium chemistry and cloud formation.
- **Magnetic Field:** This is a good approximation when modeling the neutral photosphere (where most of the emitted flux emerges) of low mass, very low mass stars, and brown dwarfs — with the exception of the ultraviolet and visual spectral range of flaring stars and for the resulting emission lines.
- **Other multi-dimensional aspects**

and assumes instead that the averaged properties of stars can be approximated by modeling their properties **radially (uni-dimensionally) and statically**. In this case, the Navier-Stokes equations reduce to the so-called hydrostatic equation and constant flux approximation for the radial or z direction:

$$\frac{dP}{dr} = \chi_{\lambda} \rho \frac{d(P_{\text{gas}} + P_{\text{rad}})}{d\tau_{\lambda}} = -\rho g(r) , \quad \text{Hydrostatic equation}$$

$$\frac{\partial F_{\text{rad}}}{\partial r} = \frac{\partial (\int F_{\lambda} d\lambda)}{\partial r} = 0 , \quad \text{Constant flux approximation}$$

where  $\chi$  is the extinction coefficient (absorption + scattering i.e.  $\kappa + \sigma$ ),  $\tau$  the optical depth ( $\equiv \chi \rho dr$ ), and  $P_{\text{gas}}$  and  $P_{\text{rad}}$  the gas and radiative pressures, respectively. Instead of assuming zero motions, we average the Navier-Stokes equations over x, y, and time to obtain a statistically stationary solution, leading to an additional pressure term called dynamical or micro-turbulent pressure  $P_{\xi}$  that must be added to the pressure budget above.



# PHOENIX

Created in 1994 in Phoenix, AZ  
Peter Hauschildt, France Allard & Eddie Baron

*Allard & Hauschildt, ApJ 445, 443 (1995)*



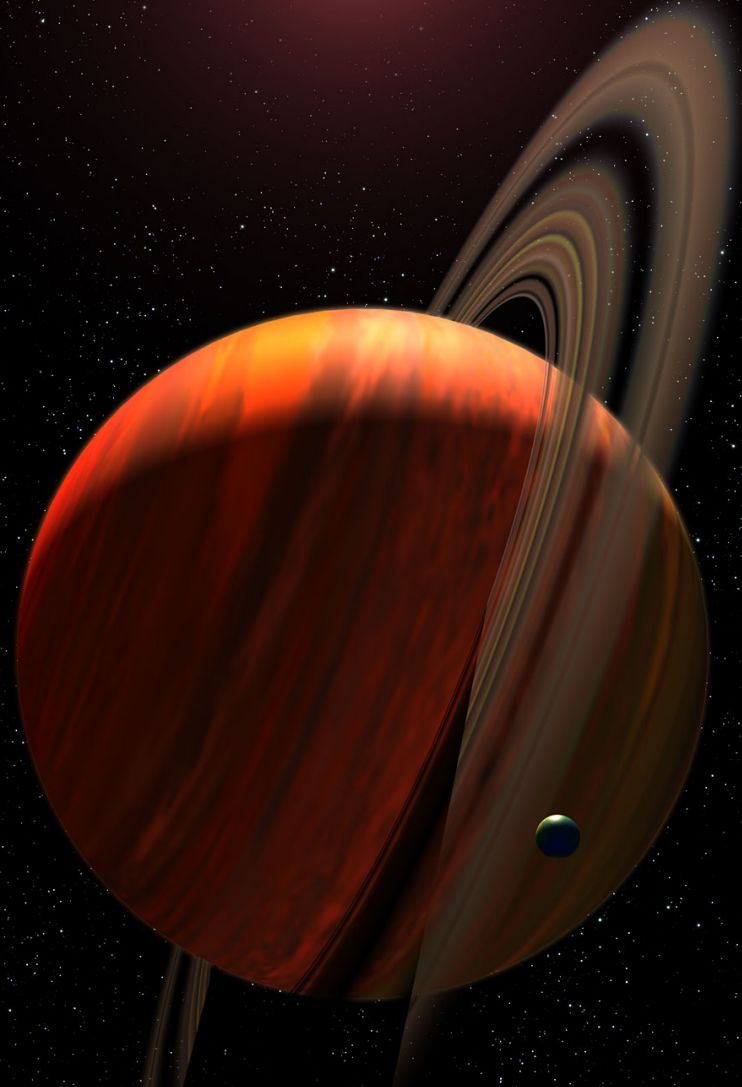
- 1D, static, Radiative Transfer OS/ALI :
  - spherical symmetry with adaptive angular resolution
  - restraint relativity effects (solution in comoving frame)
  - 3D
- **Hydrostatic Equilibrium** (stars, brown dwarfs, planets), or
- Velocity field in relativistic expansion (novae, supernovae)
- Layer-dependant velocity up to speed of light (novae, supernovae)
- **Convection**: Mixing Length Theory
- Atomic diffusion
- Non-LTE (rate-operator splitting) for atoms and CO
- **Chemical Equilibrium** with NLCE for certain species (CO, CH<sub>4</sub>, NH<sub>3</sub>)
- **26 ionization levels, 85 elements (Th, U), 600 molecules, >1000 grain types**
- **Dynamical (no pre-tabulation) Opacity Sampling**
- **Database of atomic and molecular transitions**
- **Layer-dependant Micro-Turbulence velocity** from Radiative HydroDynamic (RHD)
- **Quasi-molecular line alkali profiles**
- **Extinction cross-sections for 56 types of grains**
- **Cloud Model** based upon Rossow (1978) timescales (sedimentation, condensation)
- Supersaturation computed from chemical equilibrium precomputations.
- Mixing from Radiative HydroDynamic (RHD)



# The search for planets around M dwarfs

M dwarfs comprise 75% of the stars in our Galaxy, including many nearby stars.

- Smaller planets
- $0.5 R_{\odot}$  and  $0.1 M_{\odot}$
- Easier to detect by RV, transit

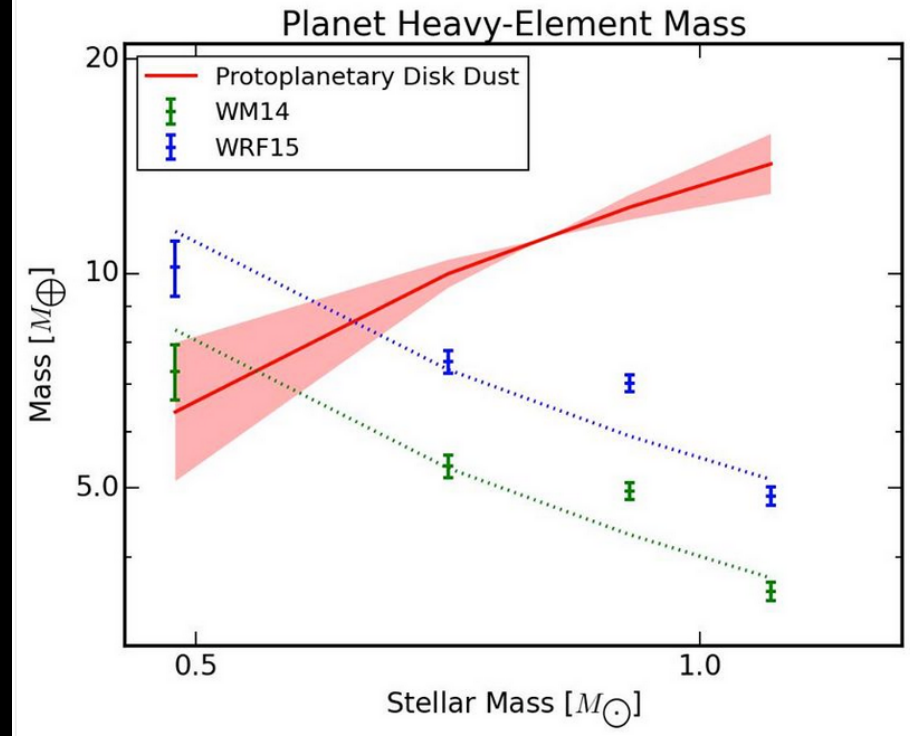


# Why do low-mass stars have more planets?

## KEPLER RESULTS

Figure 8 of Mulders et al. (2015). Average heavy-element mass locked up in planetary systems observed by Kepler versus the median stellar mass in each spectral type bin. The WRF15 mass-radius relation yields higher masses than WM14, but both relation show the same trend with stellar mass. The green and blue dotted line shows a power-law relation inversely proportional to stellar mass. The red line shows how the median dust disk mass from millimeter-wave observation scales with stellar mass, based on  $M_d \approx 0.004\% M_*$  by Andrews et al. (2013). The shaded region shows the 1 $\sigma$  confidence limit on the stellar-mass-dependent scaling of disk mass with stellar mass, and does not reflect the uncertainties in the absolute values nor the dispersion at a given stellar mass.

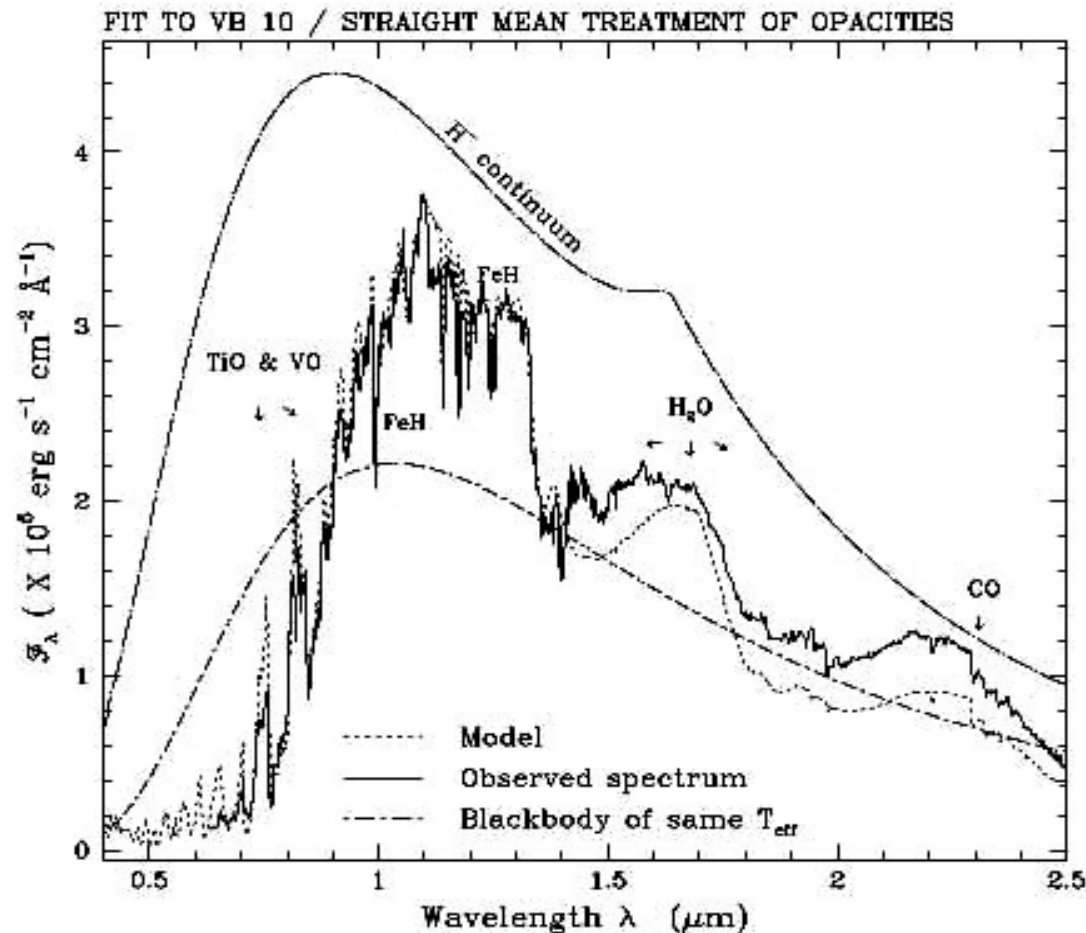
*Mulders et al. (2015)*



Sample	$T_{\text{eff}}$ [K]	$M_*$ [ $M_\odot$ ]	$M_P$ [ $M_\oplus$ ]	$M_d$ [ $M_\oplus$ ]
M	2400...3865	0.42	$7.3 \pm 0.7$	7
K	3865...5310	0.73	$5.4 \pm 0.2$	12
G	5310...5980	0.91	$5.0 \pm 0.1$	15
F	5980...7320	1.08	$3.6 \pm 0.1$	18

**Table 2**  
Planet Heavy-Element Mass per Spectral Type. Average heavy-element mass of Kepler planetary systems ( $M_P$ ) per spectral type bin, compared to median host star mass ( $M_*$ ) and protoplanetary disk dust masses ( $M_d$ ) in Taurus estimated from millimeter-wave continuum observations ( $M_d = 4 \cdot 10^{-5} M_*$ ) by Andrews et al. (2013).

# Allard & Hauschildt (1995)



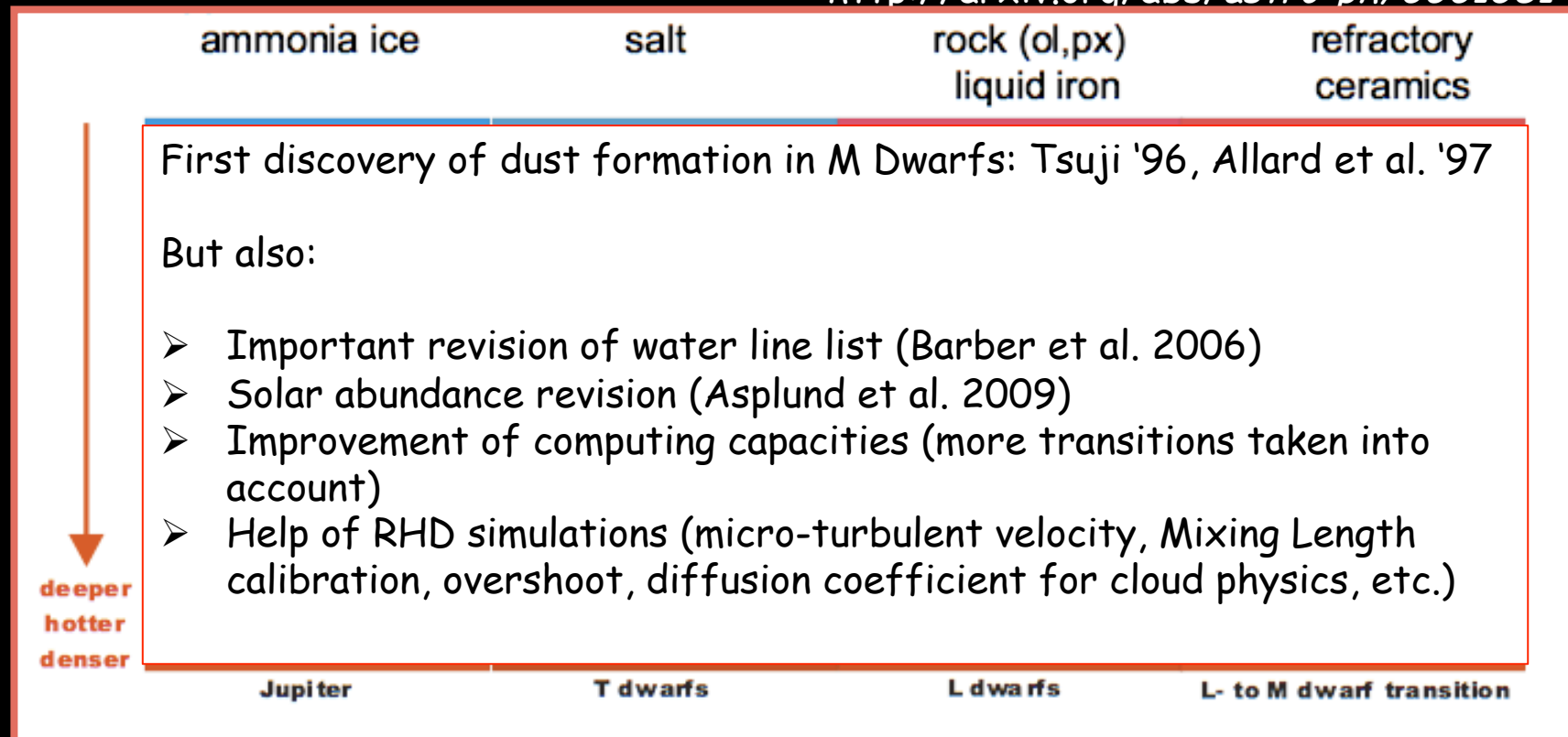
- No wavelength window onto the continuum
- Peak of SED fixed @  $1 \mu\text{m}$
- SED very different from  $\text{BB}_{\lambda}$
- Metal depletion leads to double-metals rapid depletion and discrete absorption line large wings forming from the higher pressure inner photosphere

Spectral Energy Distribution (SED) of a typical Very Low Mass star (VLMs) of effective temperature ( $T_{\text{eff}}$ ) similar to that of a young brown dwarf (few million years). The SED of de dM8e VB10 (full line) is compared to a model (AH95, dotted lines) based on band model opacities. The spectrum where all discrete opacities (atomic & molecular line transitions) are omitted (dot-dashed), and the blackbody SED of same  $T_{\text{eff}}$  indicates the importance of “non-grey” opacities.

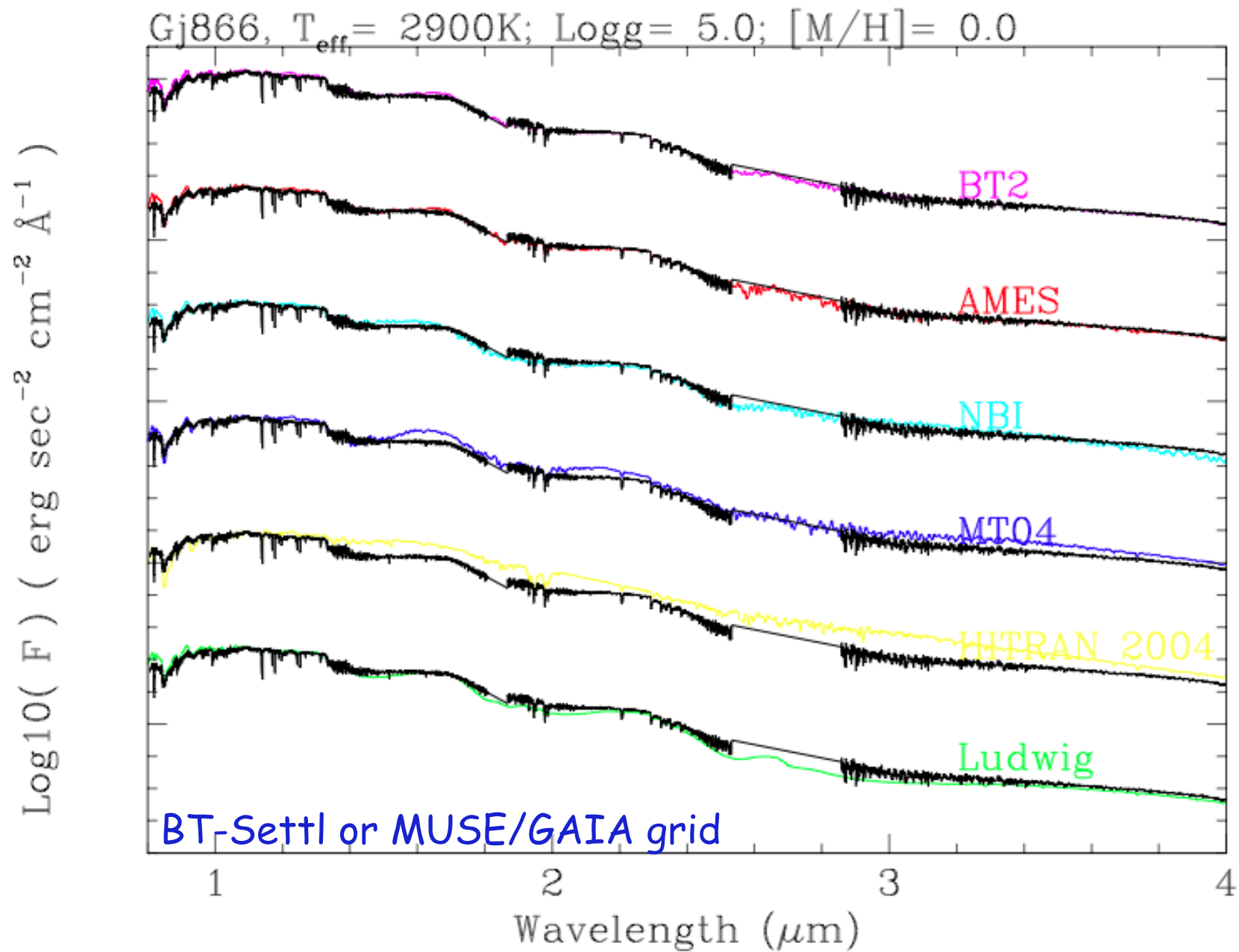


# Clouds from below $T_{\text{eff}} = 2900\text{K}$

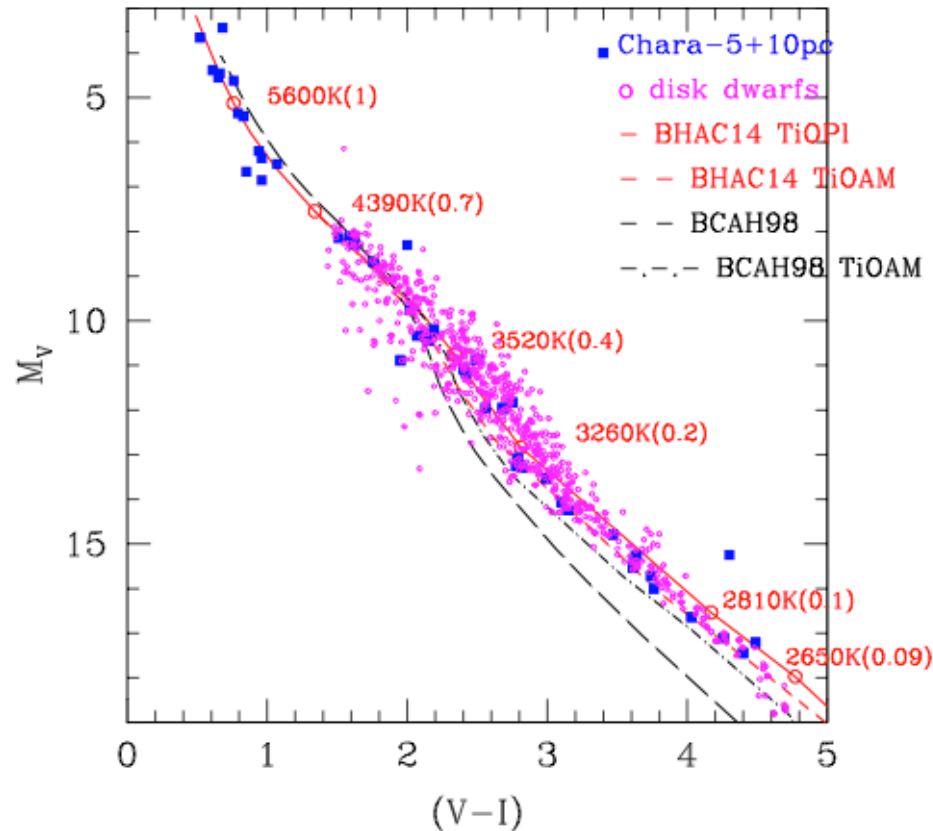
<http://arxiv.org/abs/astro-ph/0601381>



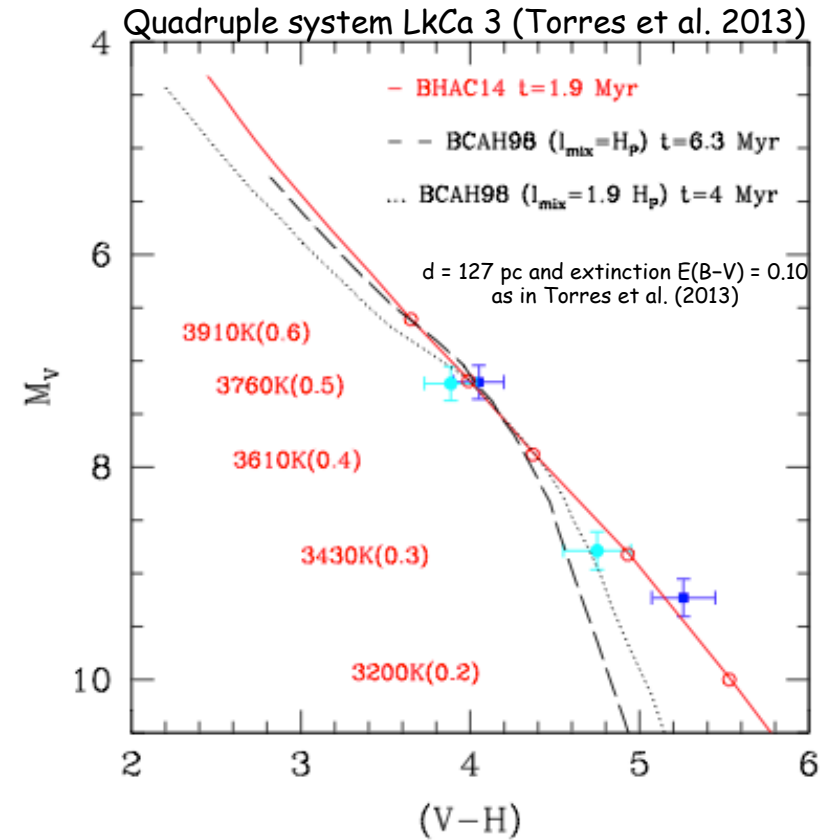
*Fergley & Lodders, Astrophysics Update 2,  
edited by John W. Mason. ISBN 3-540-30312-X.  
Published by Springer Verlag, Heidelberg, Germany, 2006, p.1*



# New BT-Settl Isochrones



Incertainties on TiO opacities remain:  
AMES TiO less accurate but more complete  
vs Plez 2008 TiO more accurate but not  
complete enough

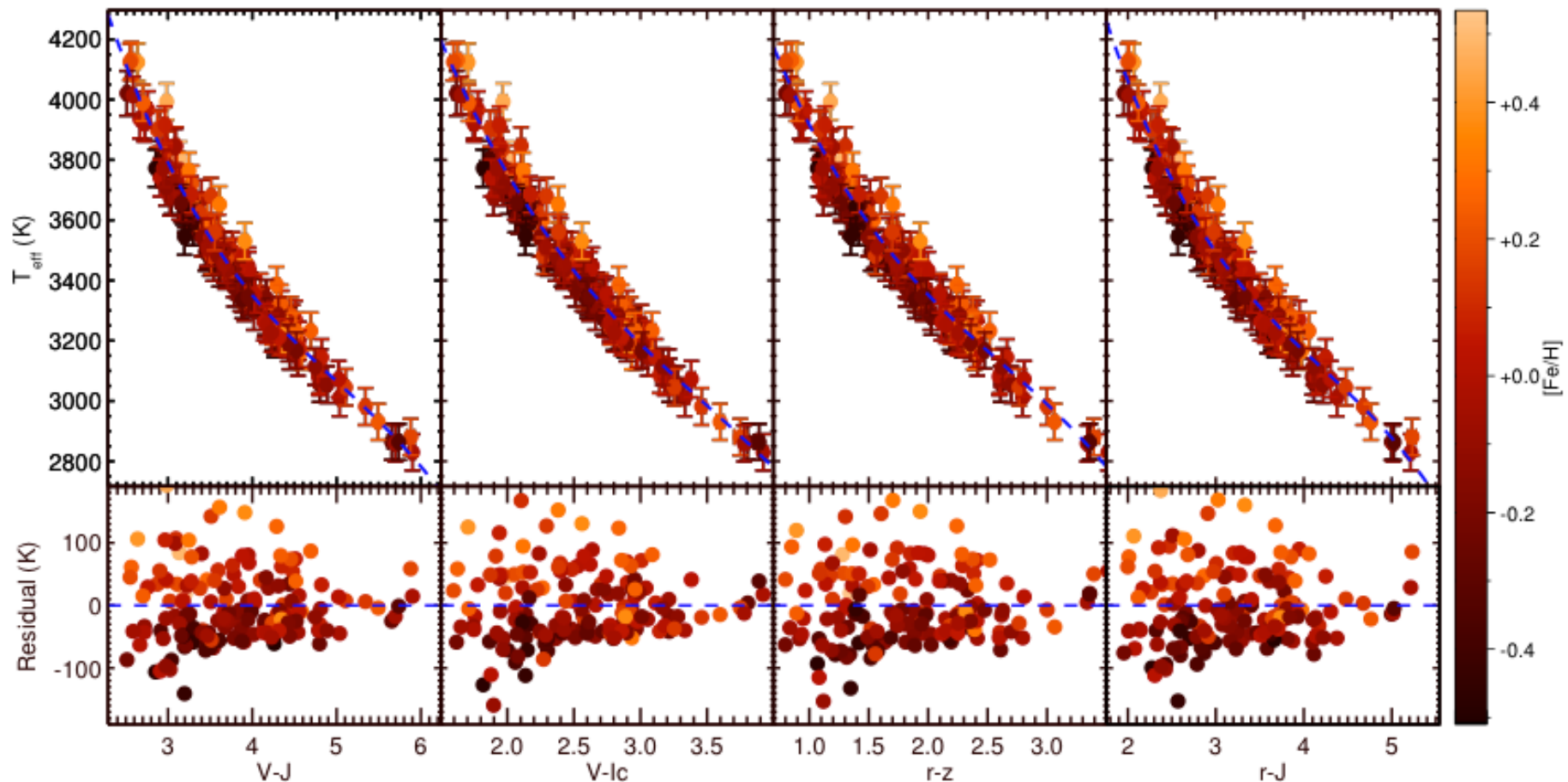


ML calibration improve the models  
for young stars, BDs & Exoplanets



# Mann et al. (2015) confirm theory!

## 160 Benchmark M Dwarfs ( $T_{\text{eff}}, \theta, R, [\text{Fe}/\text{H}]$ )





# M Subdwarfs classification

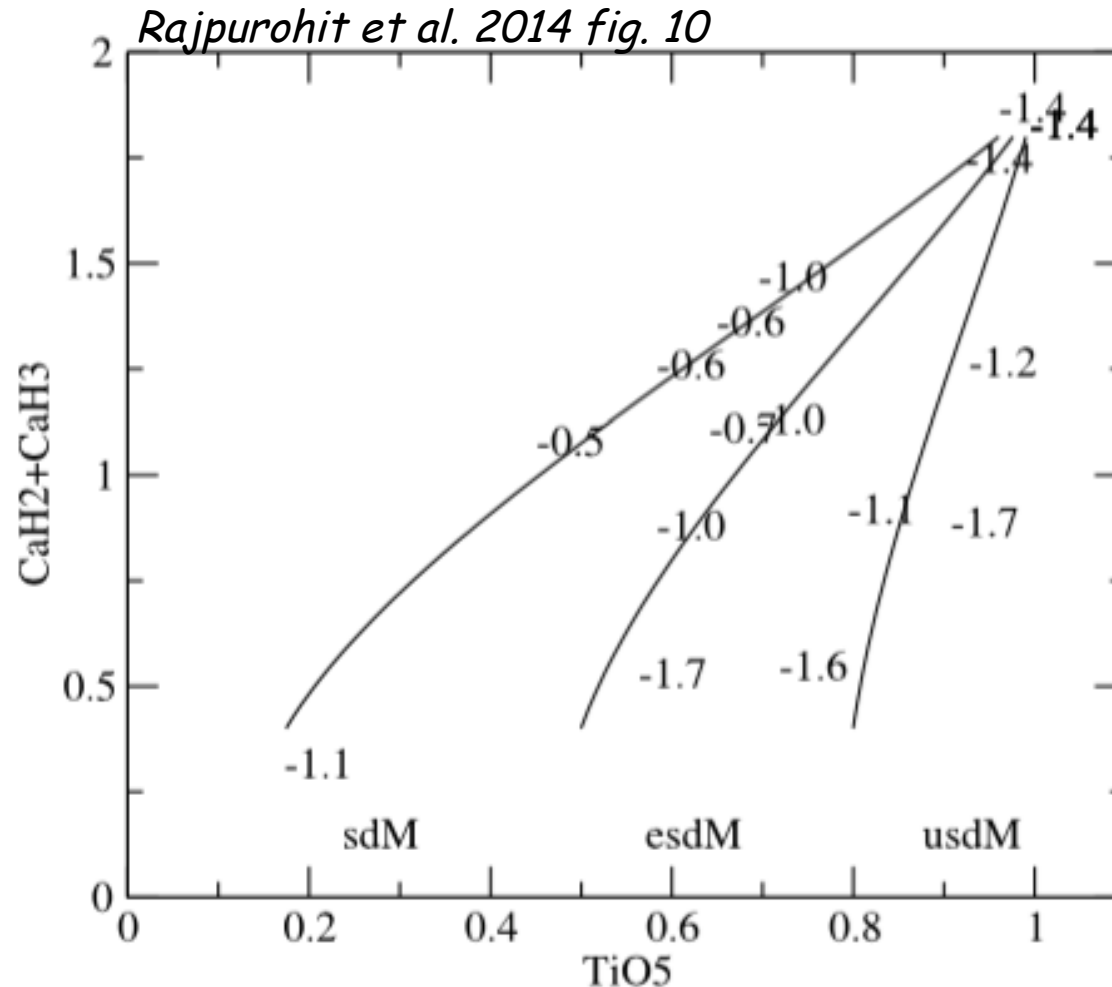
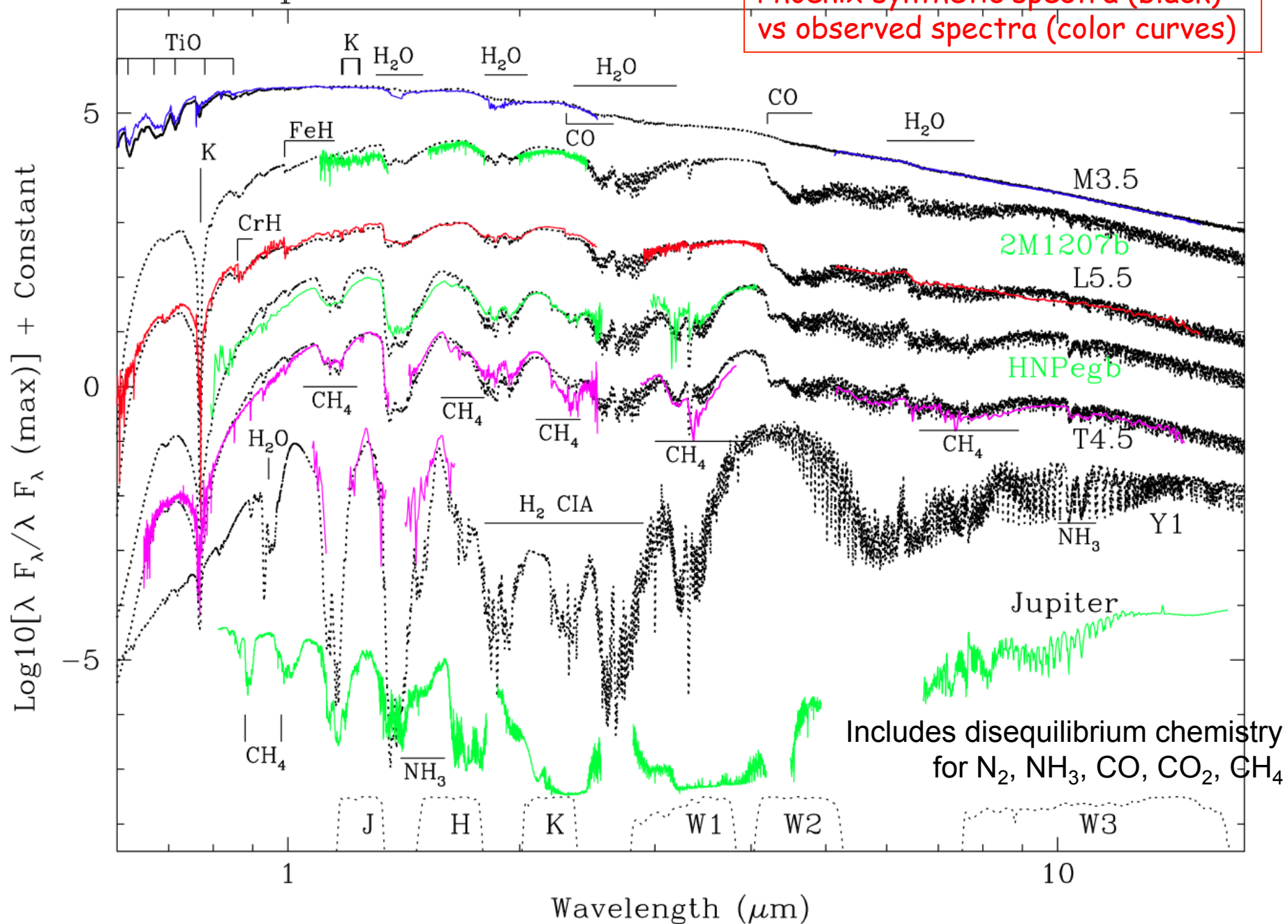


Fig. 10: CaH2+CaH3 versus TiO5 diagram for our sample. The labels indicate our metallicity determination. The lines are defined by [Lépine et al. \(2007\)](#). They show the different regions in the diagram where sdM, esdM, and usdM stars are expected to be.



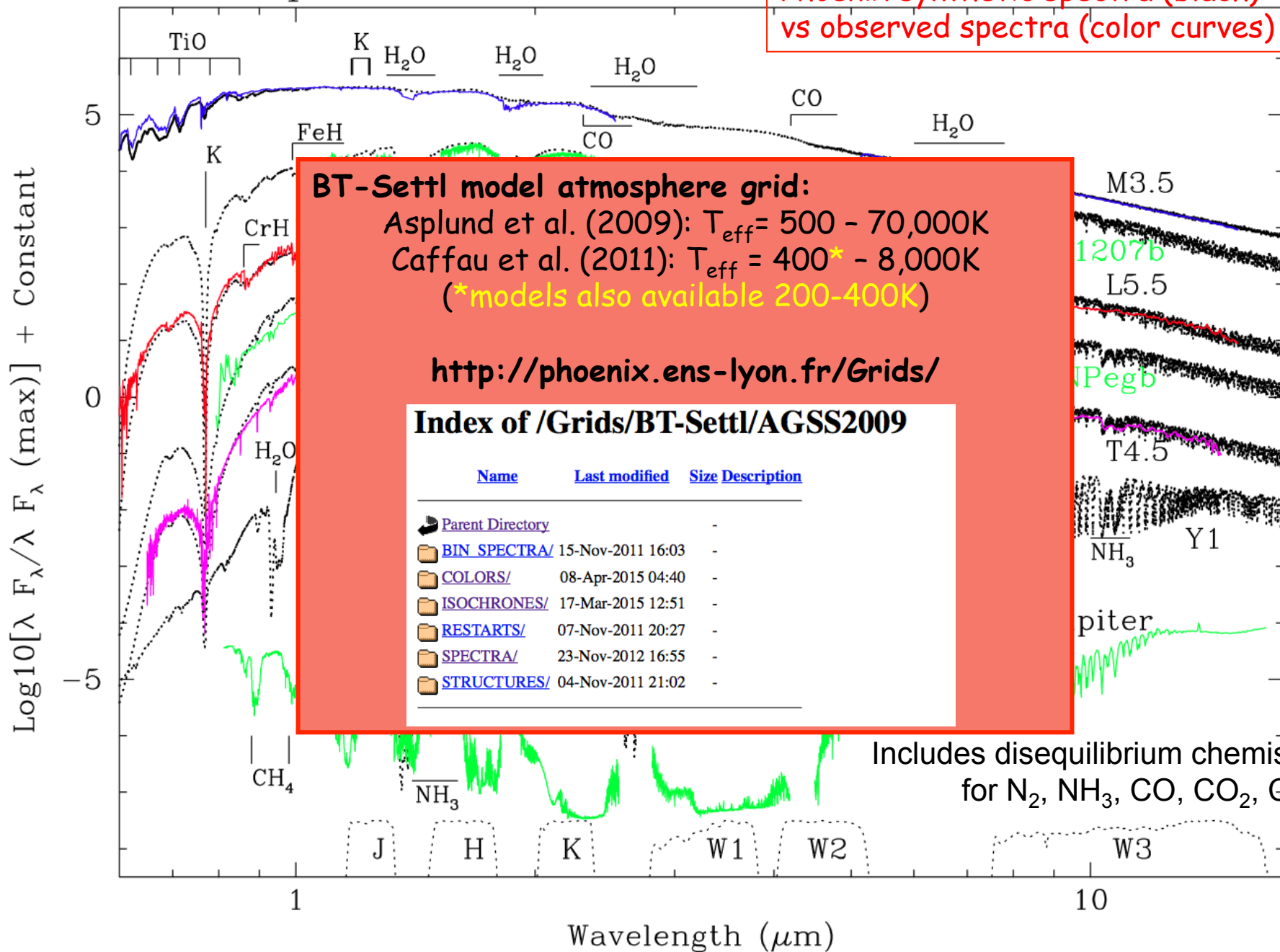
# MLTY Spectral Transition

Phoenix synthetic spectra (black)  
vs observed spectra (color curves)



# MLTY Spectral Transition

Phoenix synthetic spectra (black)  
vs observed spectra (color curves)



# The BT-Settl parameter-free cloud model

*Allard et al. (2003, 2012, 2013)*

At each atmospheric layer the characteristic timescales for the main microphysical processes (nucleation, condensation, sedimentation) are compared to the advective mixing time scale

→ averaged grain size, composition, and number density

Solved from bottom up assuming zero depletion at the bottom and actualizing the equilibrium chemistry after sedimentation gradually from bottom to the top of the atmosphere

→ condensation history preserved

i.e. e.g. if an atomic element sediments out, grains involving this element cannot form higher up in the atmosphere where it would have long sedimented out in the history of this planet

Equations:

-Nucleation rate: cosmic rays interactions with Earth atmosphere (Tanaka 2005)

→ Allows to take into account a large number of grain types (56)

-Characteristic timescales for condensation and sedimentation (Rossow 1978)

-Diffusion coefficient from RHD simulations (Freytag et al. 2010)

-Supersaturation determined taking advantage of chemical equilibrium tables

-Log-Normal grain size distribution using the average grain size determined in each layer

-Grain opacities assuming non-porous spherical grains

-Index of refraction from the Jena database

# The BT-Settl parameter-free cloud model

*Allard et al. (2003, 2012, 2013)*

At each atmospheric layer the characteristic timescales for the main microphysical processes (nucleation, condensation, sedimentation) are compared to the advective mixing time scale

→ averaged grain size, composition, and number density

Solved from  
equilibrium  
atmosphere

## Possible Improvements:

- Pressure Limited Supersaturation
- More realistic Grain Size Distributions
- Inhomogeneous grain cross-sections
- Porosity of grains
- Revision of the mixing law of Freytag et al. (2010) based on new 3D high spatial resolution simulations by Freytag et al. (2015 in prép.)

izing the  
top of the

the atmosphere  
of this planet

Equations:

- Nucleation rate: cosmic rays interactions with Earth atmosphere (Tanaka 2005)
  - Allows to take into account a large number of grain types (56)
- Characteristic timescales for condensation and sedimentation (Rossow 1978)
- Diffusion coefficient from RHD simulations (Freytag et al. 2010)
- Supersaturation determined taking advantage of chemical equilibrium tables
- Log-Normal grain size distribution using the average grain size determined in each layer
- Grain opacities assuming non-porous spherical grains
- Index of refraction from the Jena database





Bernd Freytag, ENS-Lyon, now Uppsala  
<http://perso.ens-lyon.fr/bernd.freytag>

# CO5BOLD

COnservative COde for the COmputation of  
COmpressible CONvection in a BOx of  
L Dimensions with  $l=2,3$

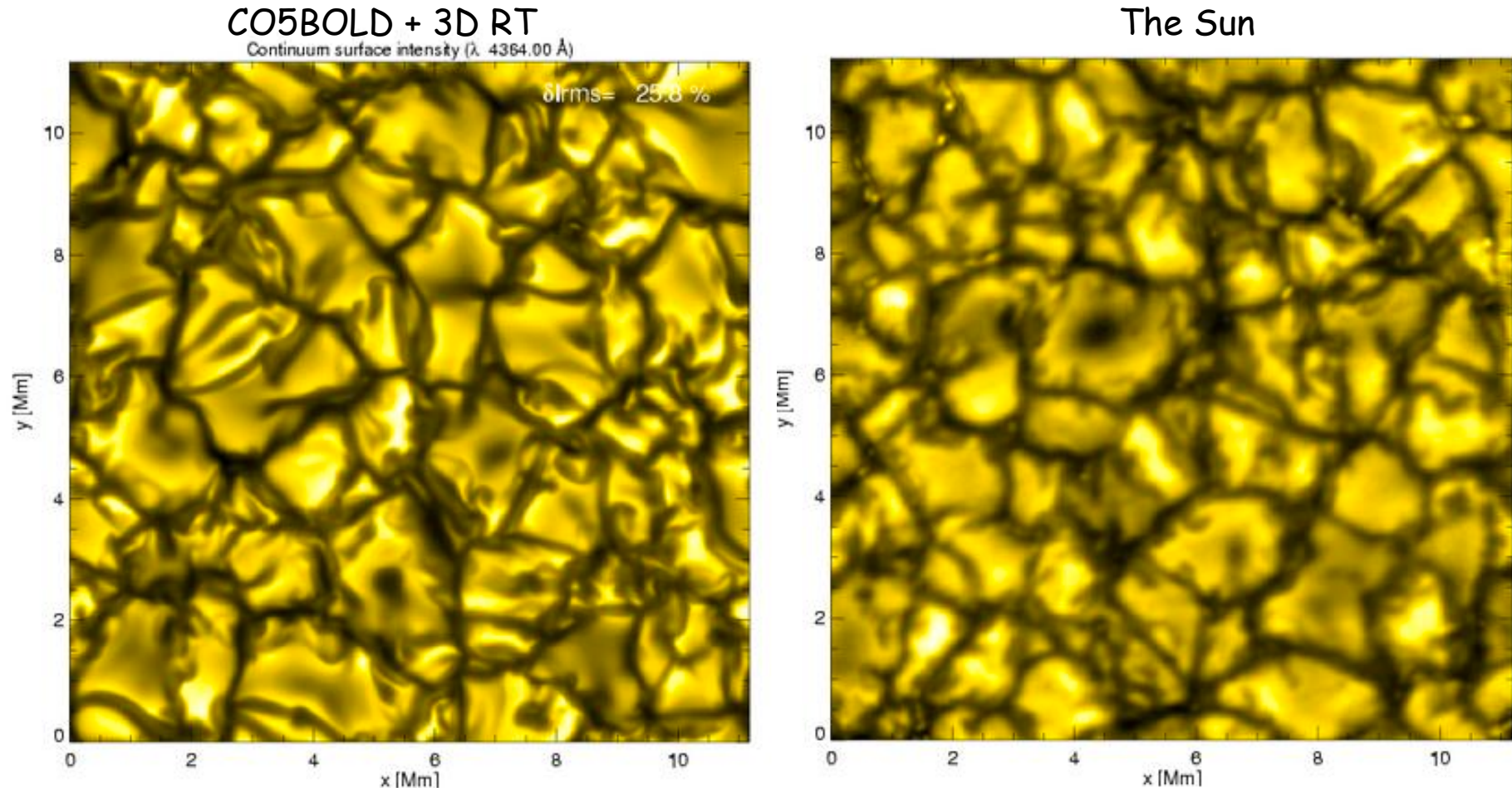
H. G. Ludwig, W. Schaffenberger,  
S. Wedemeyer-Böhm, S. Höfner, Allard, F.



Matthias Steffen, IAP  
Potsdam, Germany  
<http://www.aip.de/~mst/>

- General: 2D/3D Cartesian box, parallelized with OpenMP
- Magneto-Hydrodynamics (compressible):
  - ✓ HYD module: approximate Riemann solver (Roe type)
  - ✓ MHD module: HLLC solver
- Radiation transport:
  - ✓ Module for global "Star-in-a-Box" models (central potential)
  - ✓ Module for local "Box-in-a-Star" models (constant gravity)
  - ✓ Non-local transport, grey/non-grey opacity scheme
  - ✓ opacities from ATLAS, MARCS, PHOENIX
- Molecules, dust; additional densities:
  - ✓ Dust; 2-bin: monomers + grains, one size per grid cell, forsterite ( $\text{Mg}_2\text{SiO}_4$ )
  - ✓ Dust; multi-bin: monomers + several grain sizes, forsterite ( $\text{Mg}_2\text{SiO}_4$ )
  - ✓ Dust; 4-moment method: amorphous carbon
  - ✓ Molecules: network for CO
- Rotation: Coriolis and Centrifugal Forces in each grid cell
- Impinging radiation from a parent star

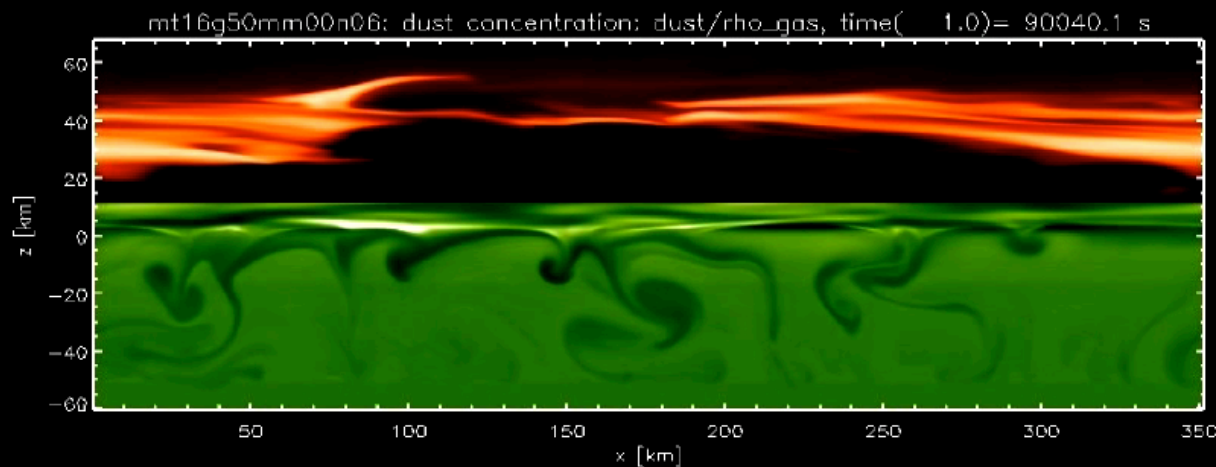
# RHD+3D RT vs Solar Granulation



Simulations with CO5BOLD by Matthias Steffen (Steffen, 2004, 2007). Observations with Swedish Solar Telescope on La Palma by the group of Mats Carlsson. Additional observables: limb-darkening, line profiles.

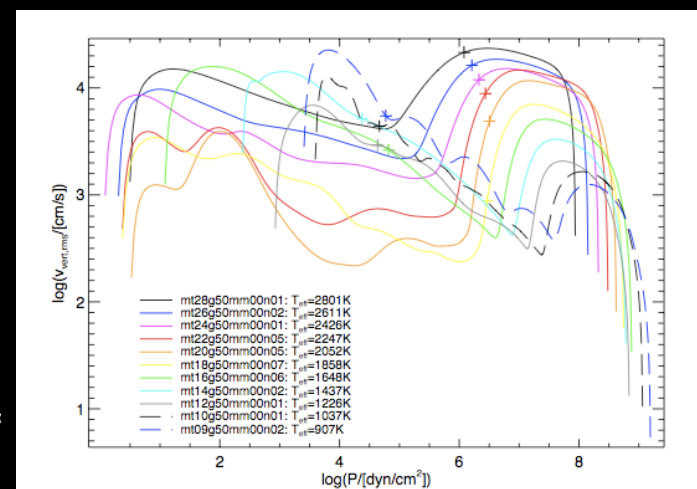
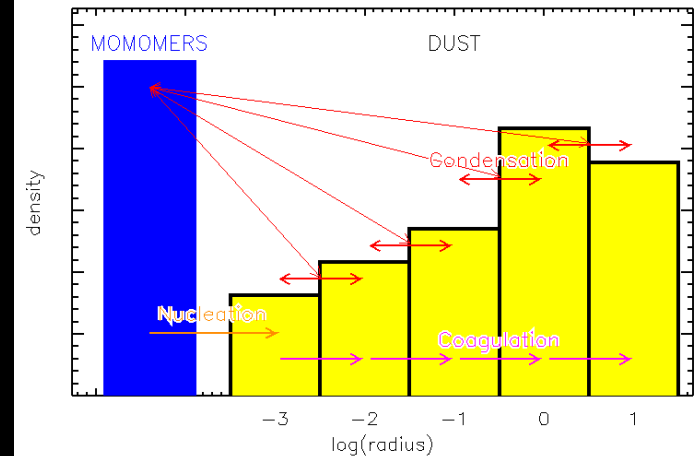
## 2D HDR simulations of the dust cloud formation in brown dwarfs atmospheres

- Clouds form a few pressure scale heights above the convection zone
- Gravity waves and convective overshoot form at the convective-radiative (or tachocline) boundary



W350 x H80 km<sup>2</sup> during 36 hrs

CO5BOLD simulations (Freytag et al. 2010) of the gas and forsterite ( $\text{Mg}_2\text{SiO}_4$ ) dust based on PHOENIX opacities, on a cloud model (dust size bin distribution), and on the nucleation, condensation, coagulation, and sedimentation rates by Rossow (1978). Shown, in red, the dust grain mass density, and, in green, the entropy indicates the entropy.

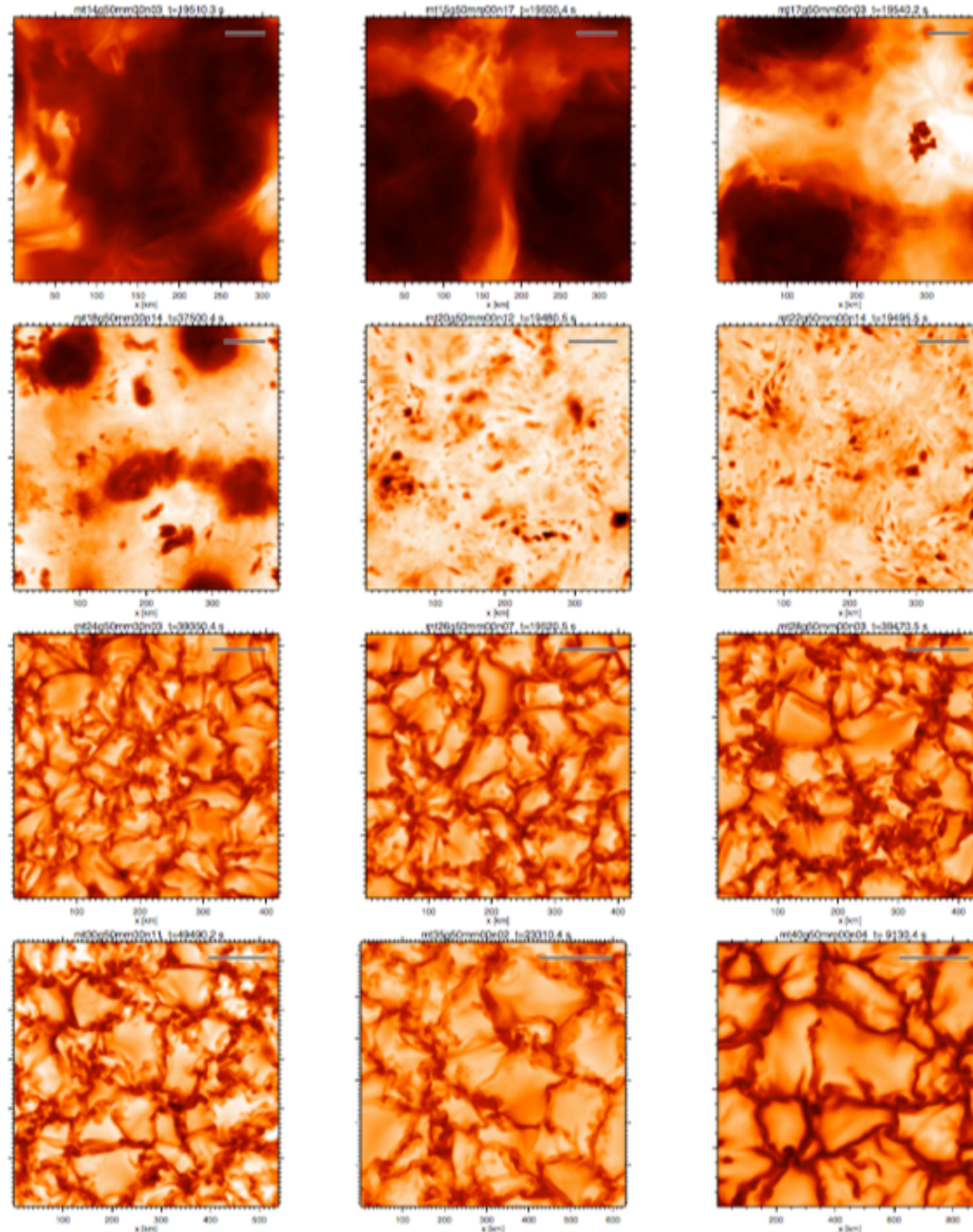




# 3D HDR simulations of M-L dwarfs

*Freytag & Allard (2015, in prép.)*

- Dust forms below 2900K
- Small-scaled clouds appear on simulation box below 2700K
- Uniform cloud layer covers the simulation below 2000K
- Clouds run with a gravity wave through de simulation box

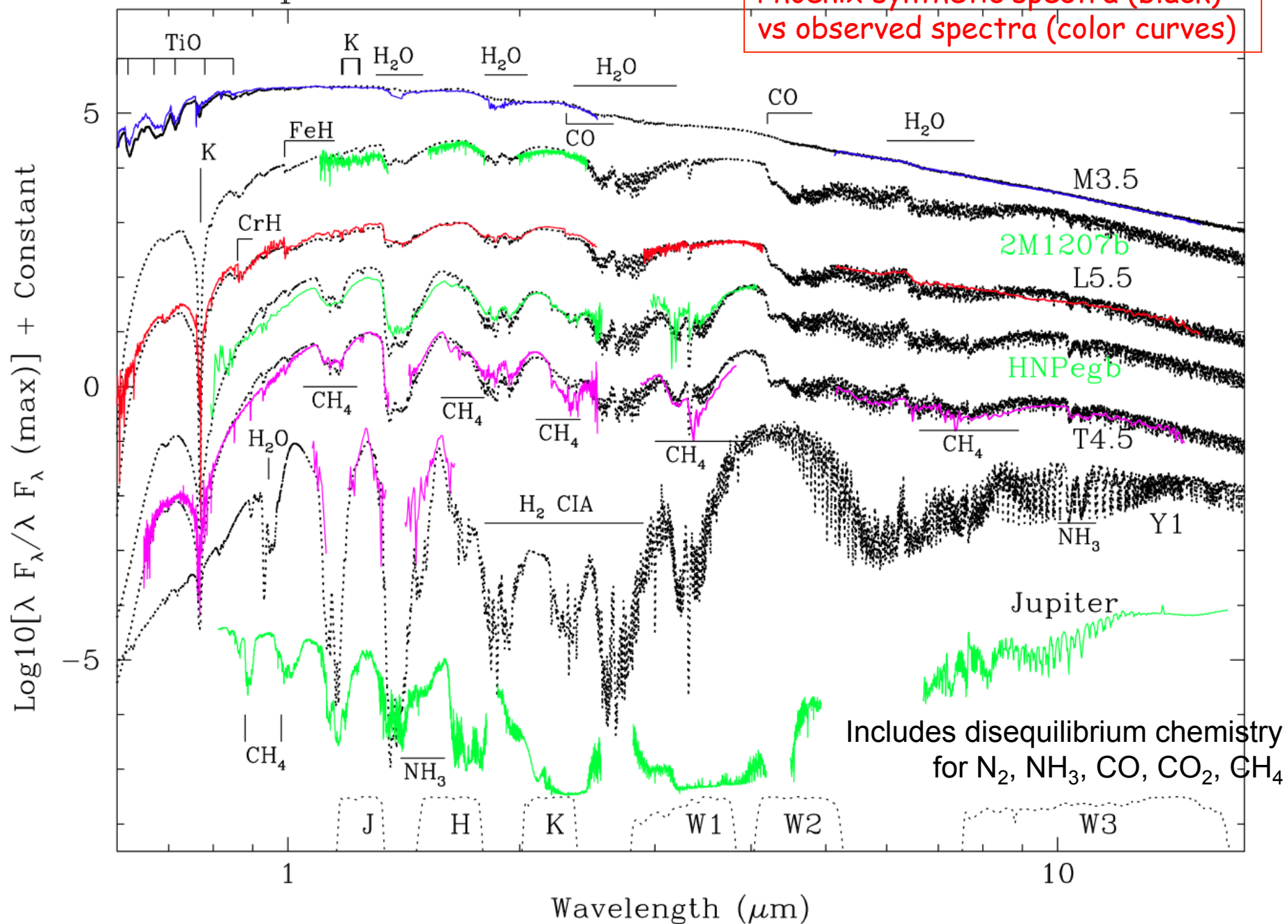


Arrêts-sur-image montrant l'intensité émergente de simulations HDR 3D de type "box-in-a-star" calculées avec CO5BOLD (Freytag & Allard, A&A en prép.) - de gauche en haut au bas à droite - les cas de  $T_{\text{eff}} = 1400\text{K}, 1500\text{K}, 1600\text{K}, 1700\text{K}, 1800\text{K}, 2000\text{K}, 2200\text{K}, 2500\text{K}, 2600\text{K}, 2800\text{K}, 3000\text{K}, 3200\text{K}, 3500\text{K},$  et  $4000\text{K}$ ,  $\log g = 5.0$ , et composition solaire. La barre dessinée sur chaque arrêt-sur-image correspond à  $10 H_p$  tel que mesuré dans la couche où  $T = T_{\text{eff}}$ , et peut être utilisée pour mesurer la taille des éléments de surface. Sous  $2200\text{K}$  la formation de nuages de forsterite ( $\text{Mg}_2\text{SiO}_4$ ) commence à modifier le contraste pour former sous  $2000\text{K}$  des ondes de gravité courantes formant des inhomogénéités de surface. La taille de ces inhomogénéités dépend donc des paramètres atmosphériques.

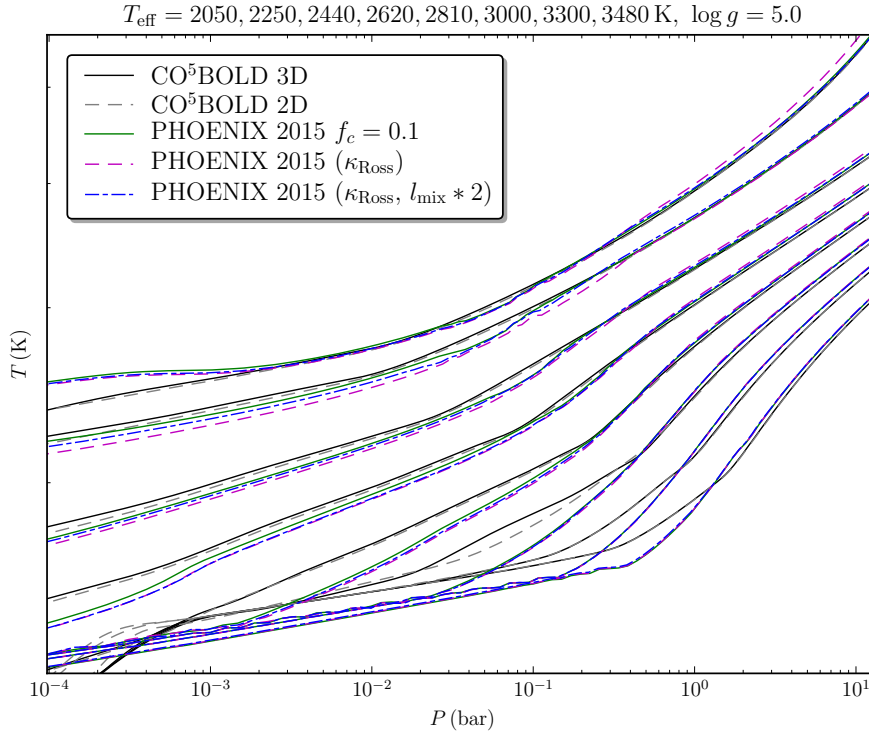


# MLTY Spectral Transition

Phoenix synthetic spectra (black)  
vs observed spectra (color curves)



# MLT: Conclusions



Adequate reproduction by the MLT of the interior T-P structure of M dwarfs (Freytag, Homeier & Allard, in prep.) when using a modification of the original Unsöld equations to reproduce the  $f_3/f_4$  value of the Mihalas (1978) formulation (Baraffe et al. 2015).

Derived mixing length  $a = l/H_p$  between 1.6 and 2.0 for M dwarfs (Baraffe et al. 2015).

**Table 1.** Characteristics of previous and present atmosphere models.

Models	Abundances	TiO	H <sub>2</sub> O	MLT variant	$l_{\text{mix}}/H_P$	$\kappa$ in $\tau_e$
NextGen <sup>1</sup>	G93 <sup>3</sup>	J94 <sup>5</sup>	M94 <sup>8</sup>	ML1	1	$\kappa_{1.2\mu m}$
Dusty/Cond <sup>2</sup>	G93 <sup>3</sup>	S98 <sup>6</sup>	PS97 <sup>9</sup>	$f_3 = 24, (f_4, f_5)$ from Eq. 2	1	$\kappa_{1.2\mu m}$
Allard et al. (2012a)	C11 <sup>4</sup>	P198 <sup>7</sup>	B06 <sup>10</sup>	$f_3 = 24, (f_4, f_5)$ from Eq. 2	2	$\kappa_{1.2\mu m}$
Present models	C11 <sup>4</sup>	P198 <sup>7</sup>	B06 <sup>10</sup>	$(f_3, f_4, f_5) = (24, 3, 1)$	$\sim 1.6\text{-}2^{11}$	$\kappa_I^{12}$

<sup>1</sup> Hauschildt et al. (1999) - <sup>2</sup> Allard et al. (2001) - <sup>3</sup> Grevesse et al. (1993) - <sup>4</sup> **DH: Asplund et al. (2009)** + Caffau et al. (2011)

<sup>5</sup> Jorgensen (1994) - <sup>6</sup> Schwenke (1998) - <sup>7</sup> Plez (1998) - <sup>8</sup> Miller et al. (1994) - <sup>9</sup> Partridge & Schwenke (1997) -

<sup>10</sup> Barber et al. (2006) - <sup>11</sup> Based on RHD calibration - <sup>12</sup> Harmonic interpolation between  $\kappa_{\text{Ross}}$  and  $\kappa_{\text{Planck}}$

# The appearance of “Brown” Dwarfs

1- Shiv S. Kumar 1963

Kumar, Shiv. S. 1963: *Models for Stars of Very Low Mass*.

NASA TN D-1907. National Aeronautics and Space Administration.

Completely convective models have been constructed for stars of masses 0.09, 0.08, 0.07, 0.06, 0.05, and 0.04 (solar units), taking into account the non-relativistic degeneracy of the stellar material. The properties of these models are presented in tabular form and in the form of graphs. It is shown that there is a lower limit to the mass of a main sequence star. The stars with mass less than this limit become completely degenerate stars or “black” dwarfs as a consequence of the gravitational contraction and therefore never go through the normal stellar evolution.



Associate Emeritus Prof.  
University of Virginia

2- Jill Tarter 1976

Tarter, Jill 1976: *Brown Dwarfs, Lilliputian Stars, Giant Planets and Missing Mass Problems*. Bulletin of the American Astronomical Society, Vol. 8, p.517. NASA Ames Research Center.

She considered that substellar objects must be darker than main sequence red dwarfs, hence brown dwarfs.



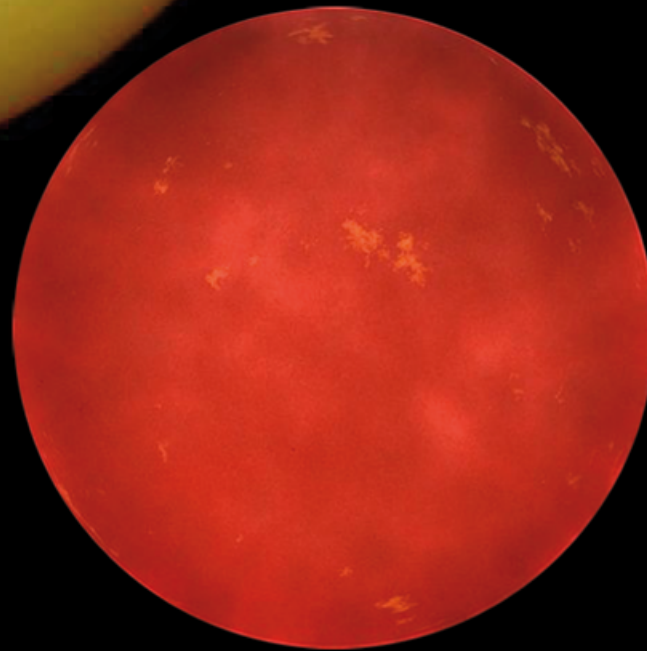
Co-Director  
Center for SETI Research  
SETI Institute  
Mountain View, CA

# The Sun with MLTY BDs & Jupiter

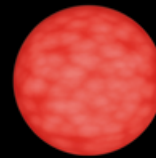
Adam Burrows  
Dept. Astrophysical Sciences  
Princeton University  
Brown dwarfs are **Magenta**



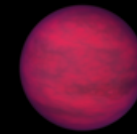
Sun



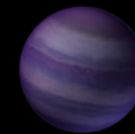
Gliese 229A



Teide 1



Gliese 229B



WISE1828



Jupiter

5,800 K

3,600 K

2,600 K

950 K

300–500 K

125 K

G2 star

red dwarf  
star

young  
brown dwarf

old  
brown dwarf

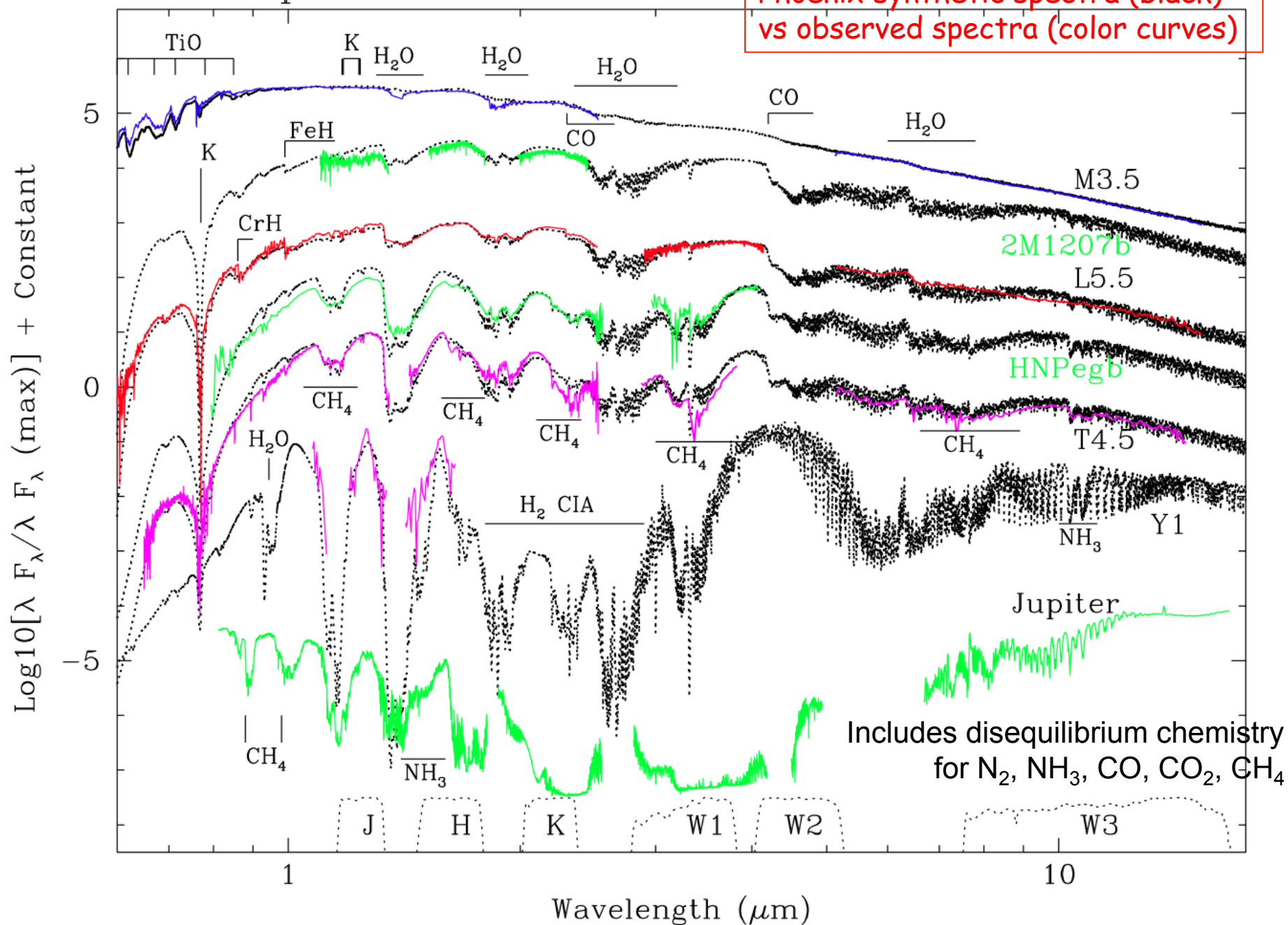
ultra-cool  
brown dwarf

planet



# MLTY Spectral Transition

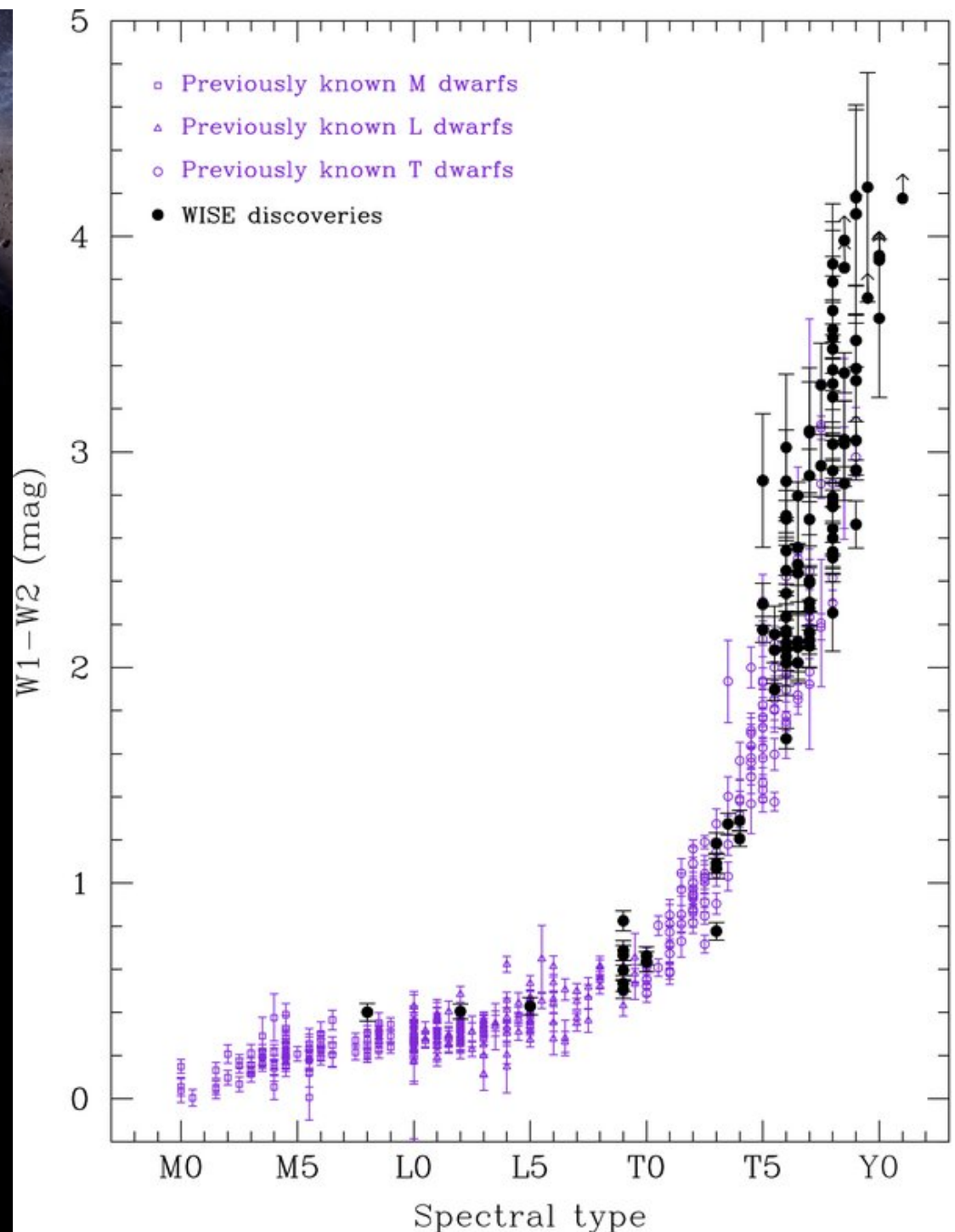
Phoenix synthetic spectra (black)  
vs observed spectra (color curves)



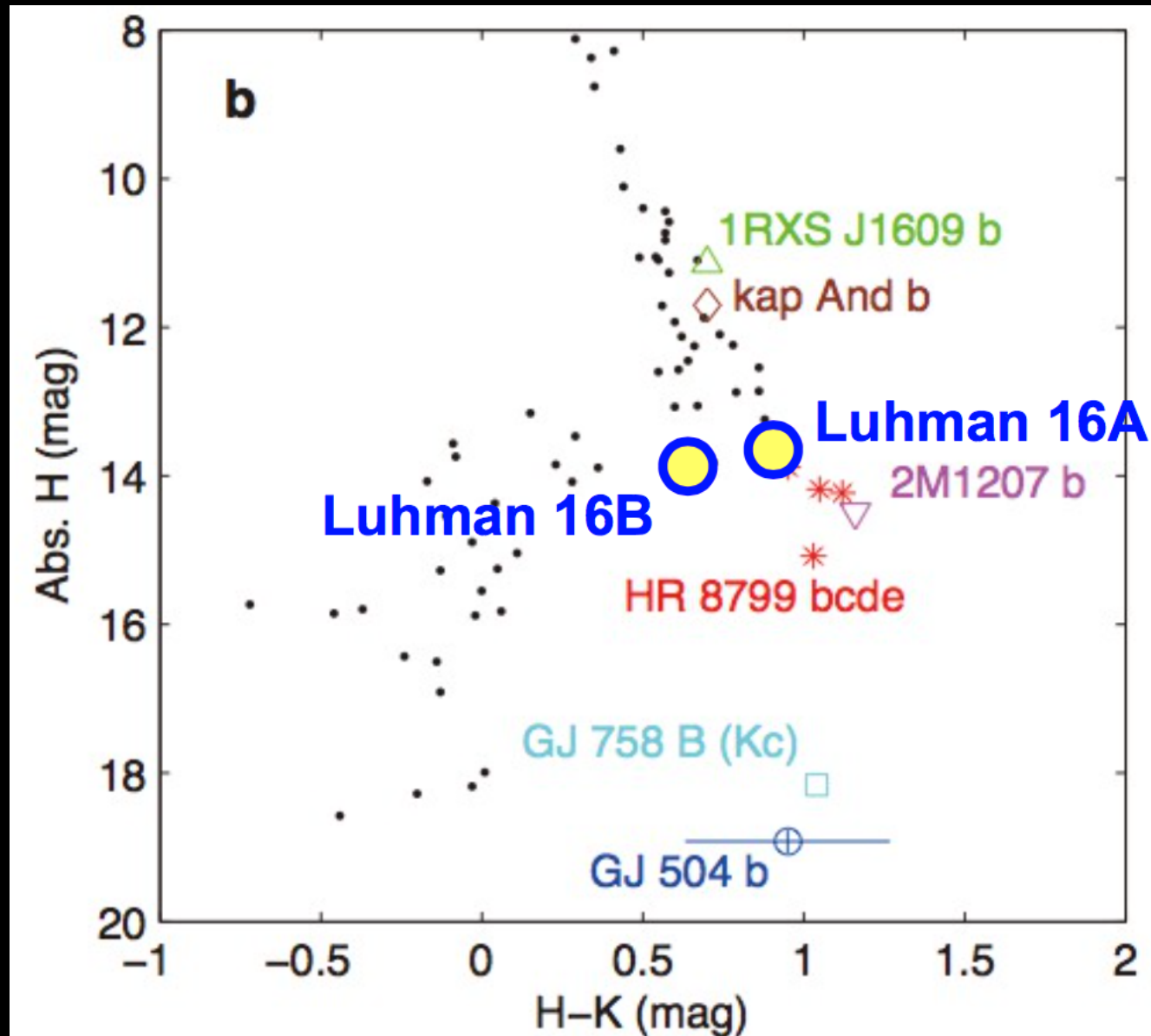
# The WISE satellite

Fg1, ApJS, vol. 406, p. 142

WISE executes a sky survey from 3 to 25  $\mu\text{m}$  with a sensibility 500,000 times that of COBE/DIRBE and hundreds of times that of IRAS. The survey helps understand the origin of planets, stars, and galaxies, and will create an infrared atlas that will become an incomparable heritage for decades to come.



# Luhman 16AB near the L/T transition



Kuzuhara et al 2013  
Kniatsev et al 2013  
Burgasser et al 2013

# Rotationally modulated variability

Recent Spitzer survey of more than 44 L3-T8 dwarfs revealed that 80% of L-type dwarfs were variable with amplitudes from 0.2 - 1.5%. It shows also that 36% of T-type dwarfs were variable with amplitudes from 0.8 - 4.6% (Metchev et al. 2014).

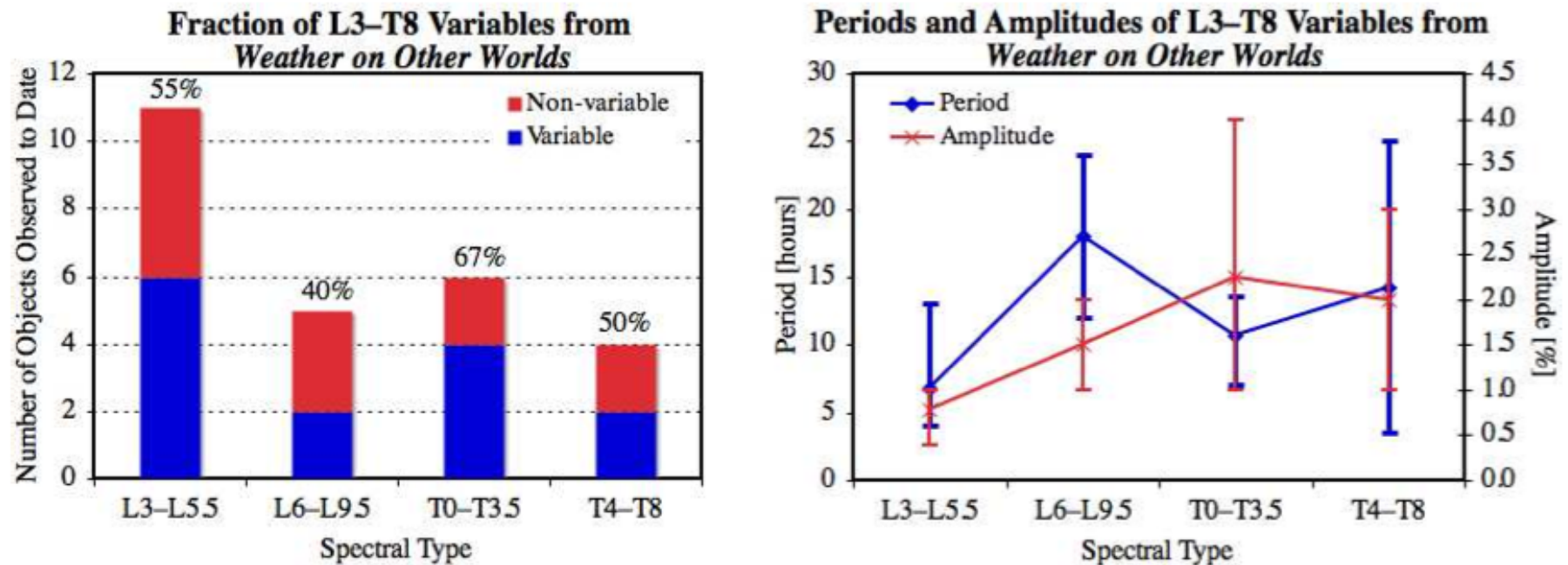


*Figure 2:* Preliminary results for the 26 observed (out of 44 total) L3-T8 dwarfs in our Cycle 8 Exploration Science program *Weather on Other Worlds*. Error bars denote the full range of observed periods and peak-to-peak amplitudes. The results demonstrate that patchy clouds are ubiquitous in 700–2000 K substellar atmospheres, and that their prominence likely continues even at cooler temperatures.

Artigau et al. (2009) were the first to detect highly significant, repeatable periodic ( $P = 2.4$  hrs,  $\Delta J = 50$  mmag) variations in a cool brown dwarf. More recently, Radigan et al. (2011) have completed the most comprehensive ground-based variability survey of L and T dwarfs, detecting highly significant periodic modulations in five out of 56 objects.



# International PhD School "F. Lucchin": Science and Technology with E-ELT

## Indirect Imaging of Ultra-Cool Dwarfs

Erice, Italie

10h00-11h00, Tuesday Oct. 13<sup>th</sup> 2015

France Allard

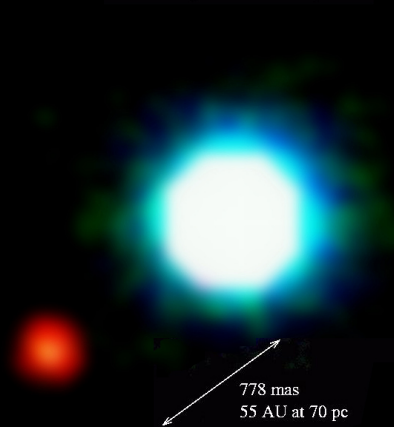
Directrice de Recherche (DR2), CNRS  
Centre de Recherche Astrophysique de Lyon  
Site ENS-Lyon



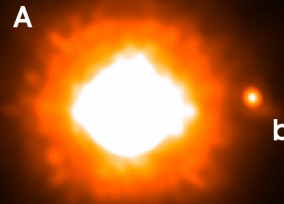
# Imaged planets

61 planets / 56 planetary systems / 3 multiple planetary systems

2MASSWJ1207334-393254



GQ Lupi



ESO VLT NACO June 2004

Neuhäuser, Guenther, Wuchterl, Mugrauer, Bedalov, Hauschildt

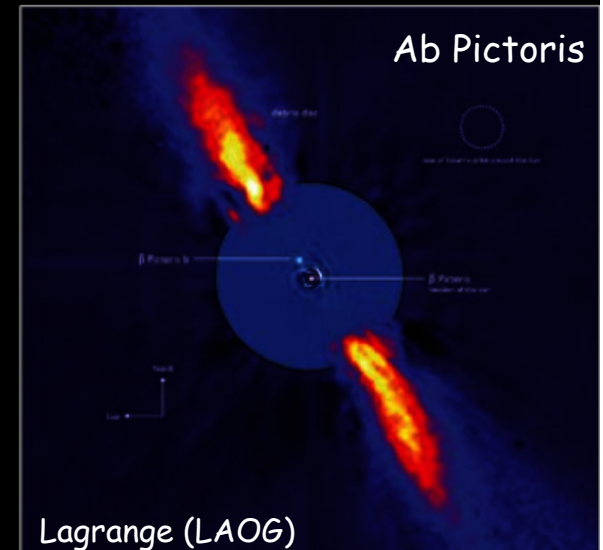


$M = 5 \pm 13 M_J$   
 $R = 1.5 R_J$   
 $a = 55 \text{ AU}$   
 $\text{age} = 8 \text{ Myr}$

$M = 20.5 \pm 21.5 M_J$   
 $R = 1.8 R_J$   
 $a = 103 \pm 37 \text{ AU}$   
 $\text{age} = 1 \pm 1 \text{ Myr}$

$M$  from isochrones

Ab Pictoris



$M = 8^{-2/+5} M_J$   
 $R = ?$   
 $a = 12 \pm 4 \text{ UA}$   
 $\text{age} = 0.012^{-0.004/+0.002} \text{ Gyr}$



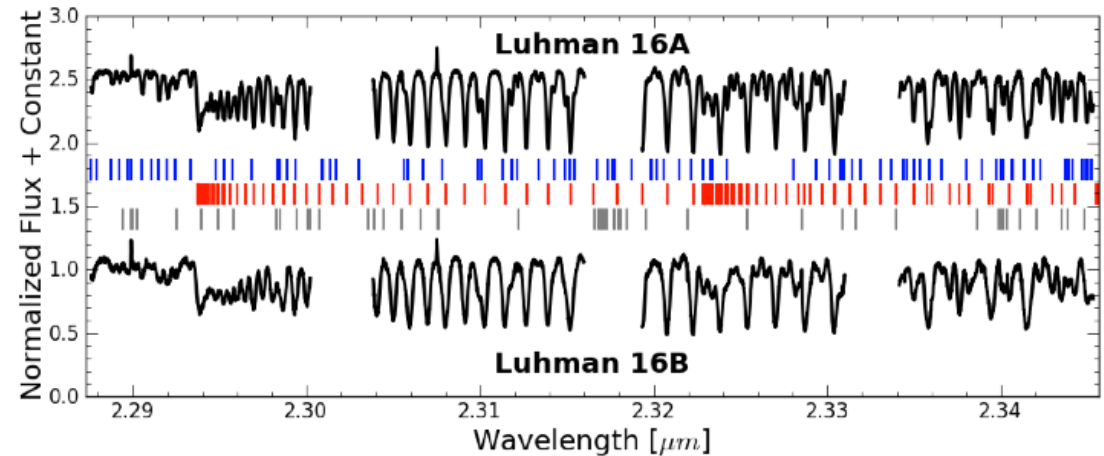
# Surface inhomogeneities revealed by Doppler Imaging!

*Crossfield et al. (Nature 505, 2014)*

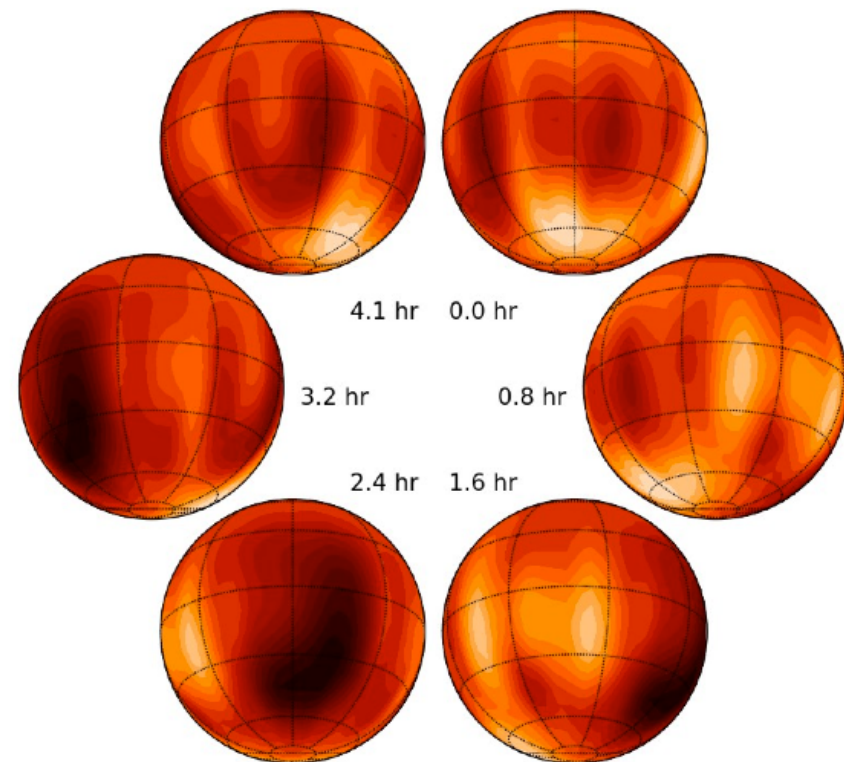
**L7.5 + T0.5 @ 2 pc**

High-resolution, near-infrared spectra of the Luhman 16AB brown dwarfs (black curves). The vertical ticks indicate absorption features: H<sub>2</sub>O (blue) and CO (red), and residual telluric features (gray). The lines of the B component are broader.

Surface map of brown dwarf Luhman 16B, which clearly depicts a bright near-polar region (seen in the upper-right panels) and a **darker mid-latitude area (lower-left panels)** consistent with large-scale cloud inhomogeneities. The lightest and darkest regions shown correspond to brightness variations of roughly  $\pm 10\%$ . The time index of each projection is indicated near the center of the figure.



CO imaging



# Outline of Next Lecture

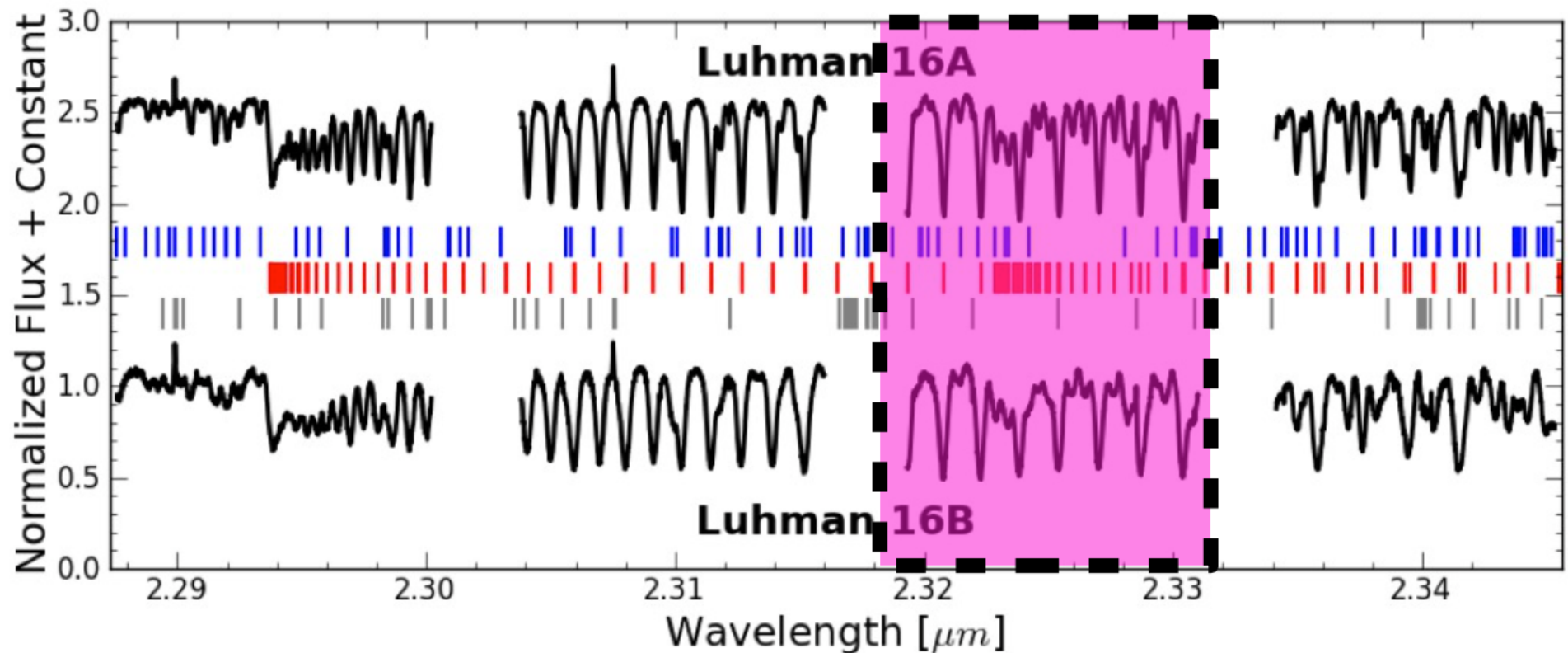
## Tuesday October 13th

- Description and Limitations of the Doppler Imaging Technique
- DI detection expectancies with CRIRES, E-ELT HIRES, JWST
- Interpretations of the patchiness of Luhman 16B
- Zeeman Doppler Imaging
- Requirements summary



# We observed Luhman 16AB with CRIRES for 5 hrs (one rotation of 'B')

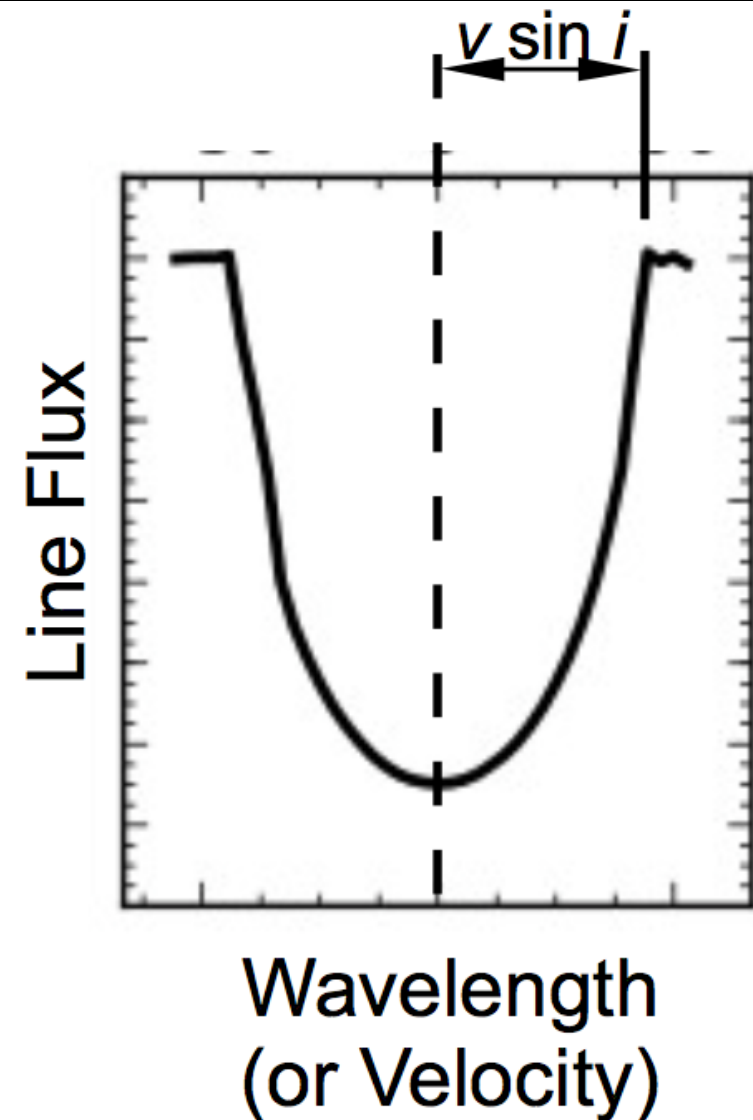
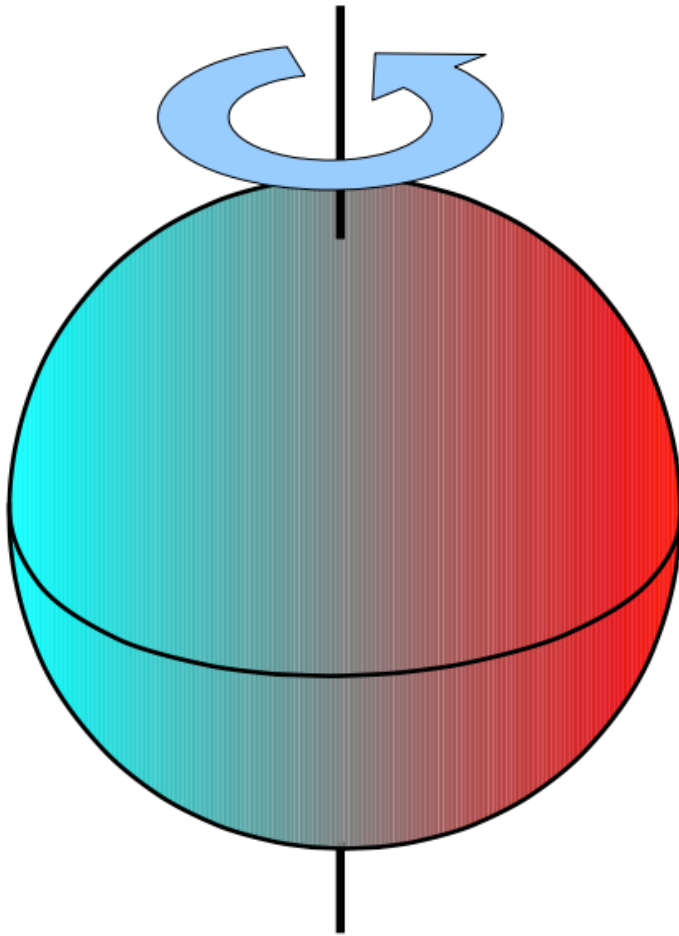
L7.5 + T0.5 @ 2 pc separated by 3 pc



*IC et al., Nature 2014*

Spectra are similar, but Luhman 16B has broader lines ( $V_{\text{sin} i} = 26 \text{ km/s}$ )

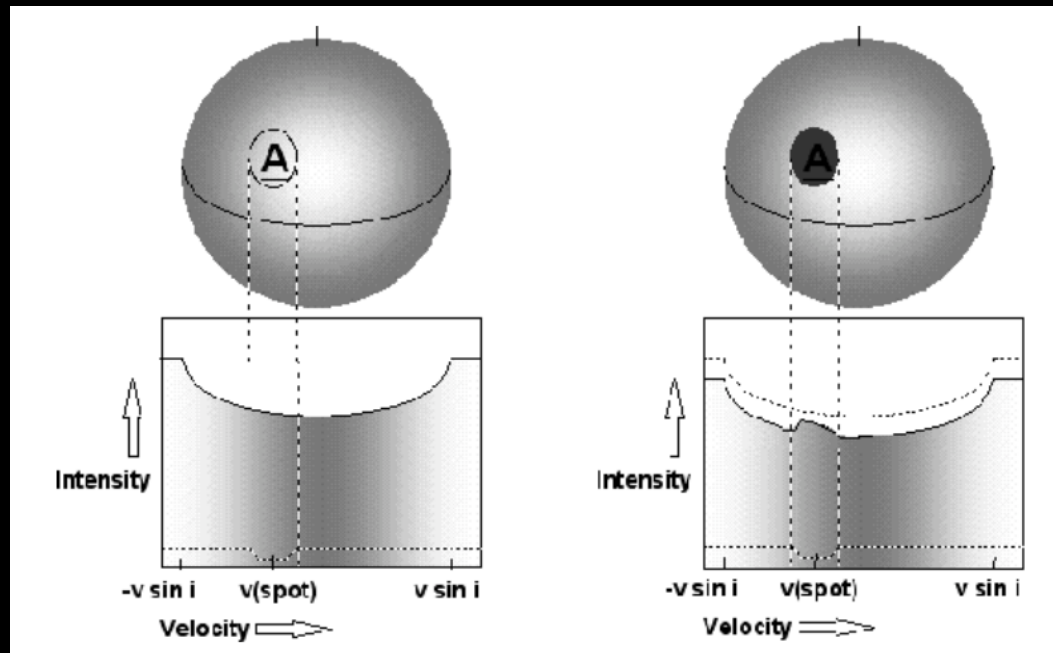
# Spectral line profiles are dominated by rotational broadening



# Doppler Imaging: history & technic

Cameron et al. (2015)

"The term ``Doppler imaging'' was coined by Vogt & Penrod (1983), who demonstrated that travelling starspot bumps were observable in the line profiles of the  $\alpha^2$ CVn HR 1099, and that an image of the stellar surface could be derived from them. A photospheric absorption line in which rotation is the dominant broadening mechanism displays time-variable irregularities if the visible surface of the star is mottled by dark spots. *As the star rotates, the spots are carried across the stellar disc, causing the bumps to change their Doppler shifts in accordance with their projected distances from the star's rotation axis.* Spots near the equator remain visible for half the stellar rotation cycle, tracing out a sinusoidal velocity variation with an amplitude equal to the stellar equatorial rotation velocity,  $V \sin i$ . Spots at progressively *higher latitudes* follow progressively *lower-amplitude* sinusoids. The fraction of the rotation cycle for which a spot remains visible depends on its latitude and the inclination of the stellar rotation axis to the line of sight. *The times at which spot signatures cross the centre of the line profile thus reveal their longitudes, while the amplitudes of their sinusoids (or equivalently, their radial accelerations at line centre) tell us their latitudes.*"



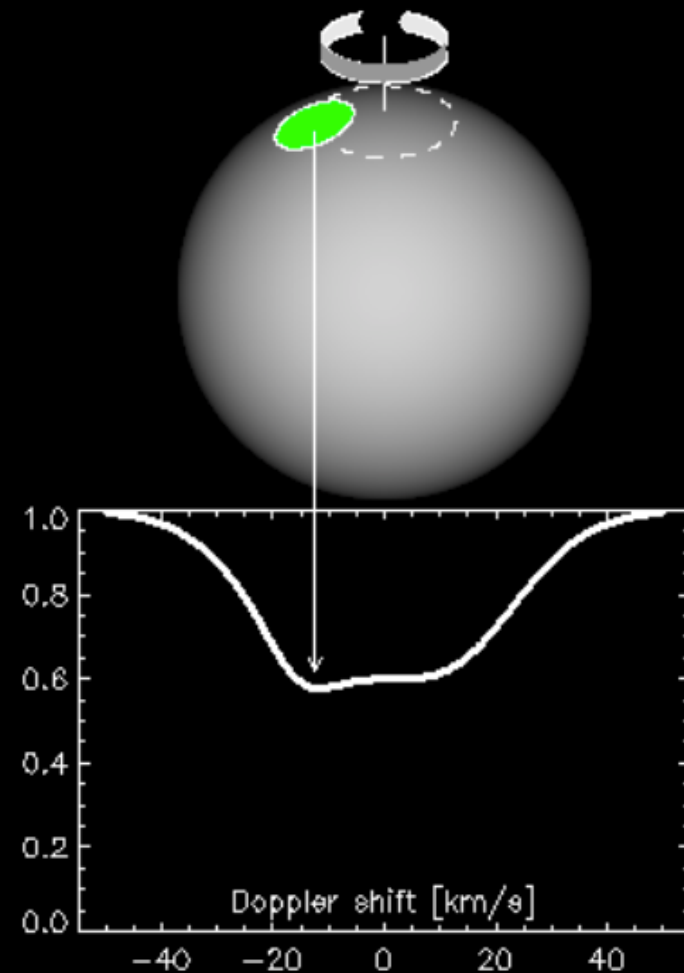
The ``missing'' light of the spot causes a diminution of the light emitted by the surface. The fact that the surface contributes to the line profile with exception of the spot causes a narrow line contribution that is Doppler shifted by an amount that depends on the projected distance of the spot from the stellar rotation axis.

The observable signature of a dark spot on the stellar surface is therefore a bright bump in every photospheric absorption line in the star's spectrum.

# Assumptions

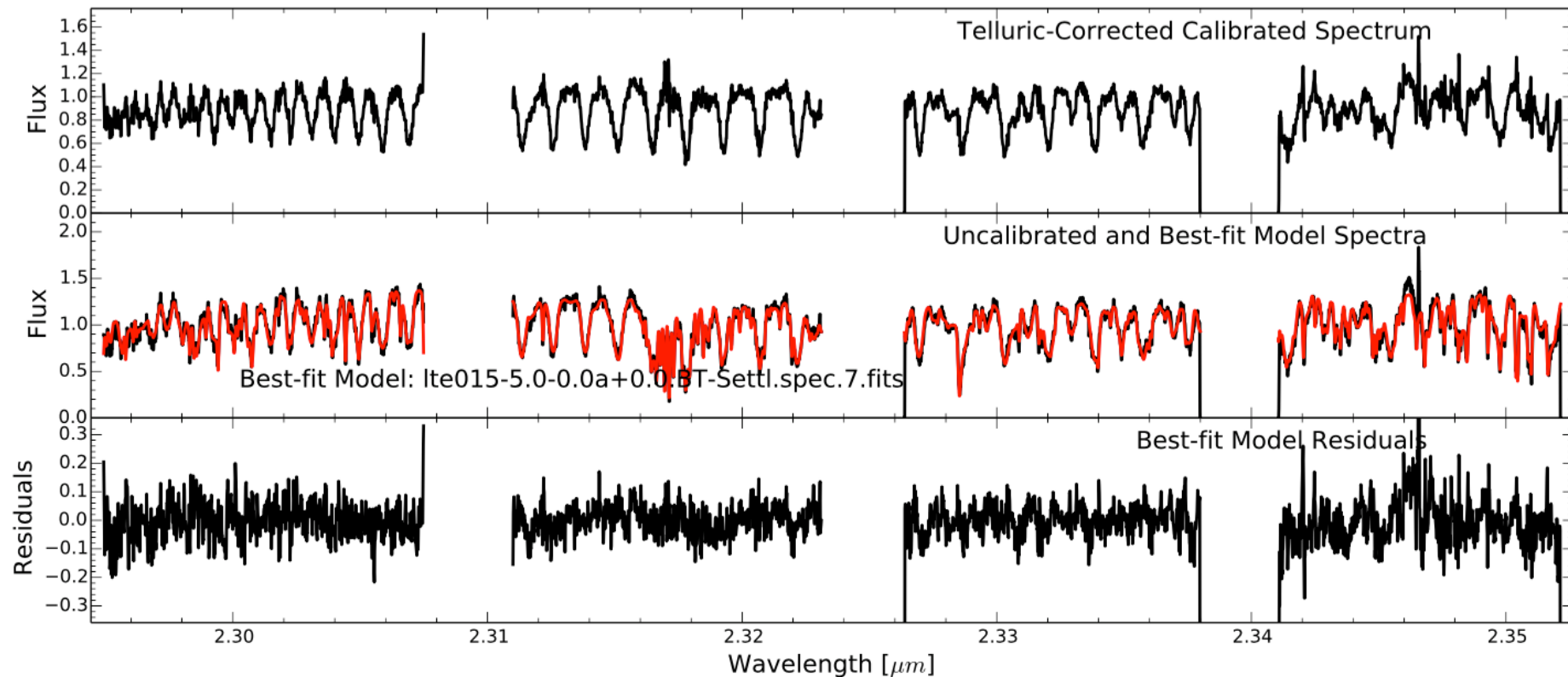
Nikolai Piskunov 2014

- Each observed spectrum is taken during the time much shorter than the rotation period.
- The surface structures do not change throughout the observing run.
- The rotational broadening is larger than the instrumental profile (profiles are resolved).
- The star rotates as a solid body (no differential rotation).
- Chemical inhomogeneities do not affect the continuum.
- The wavelength scale of observations corresponds to the stellar reference frame.





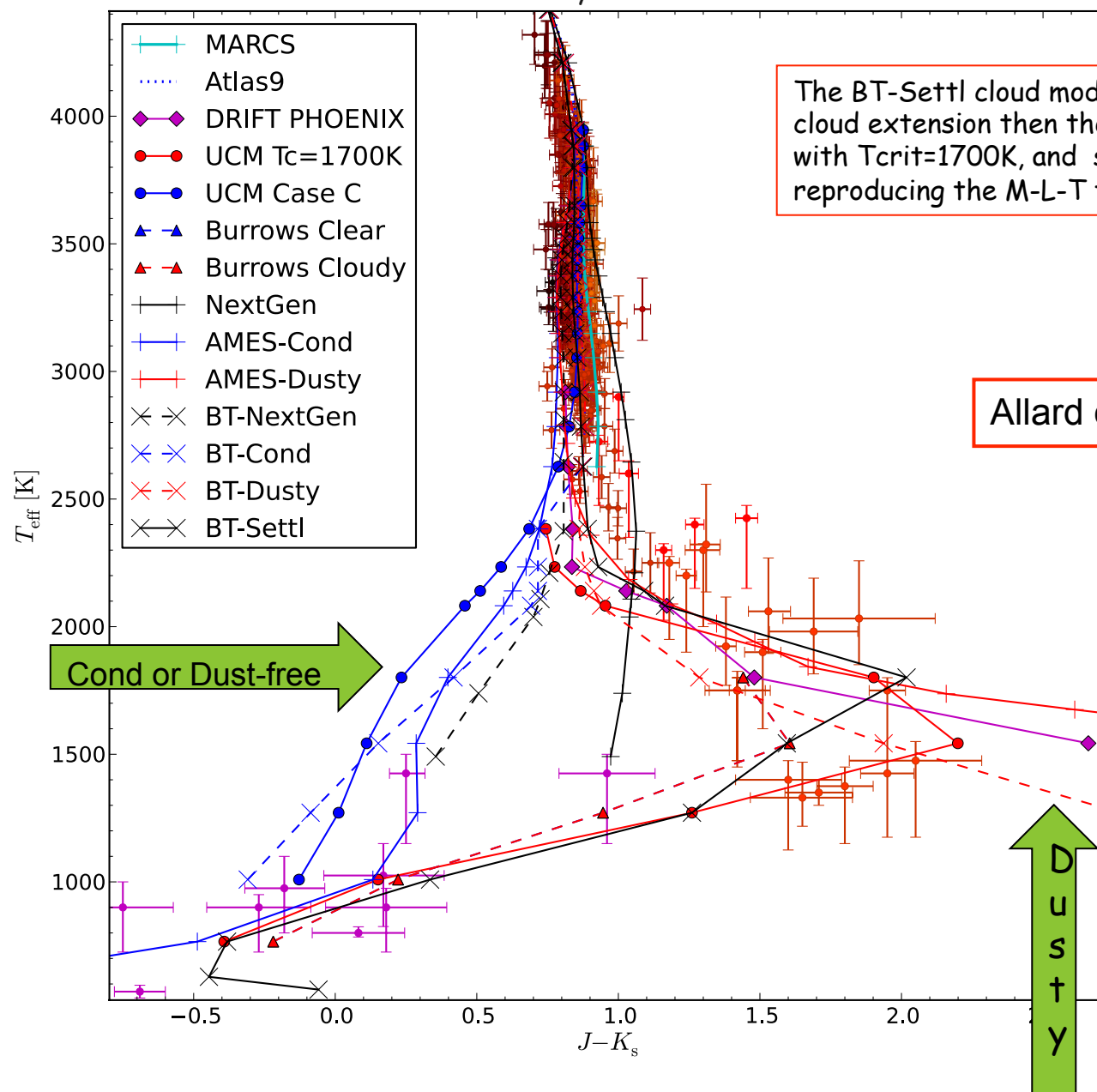
# BT-Settl model used as template against which to isolate profile features due to surface inhomogeneities



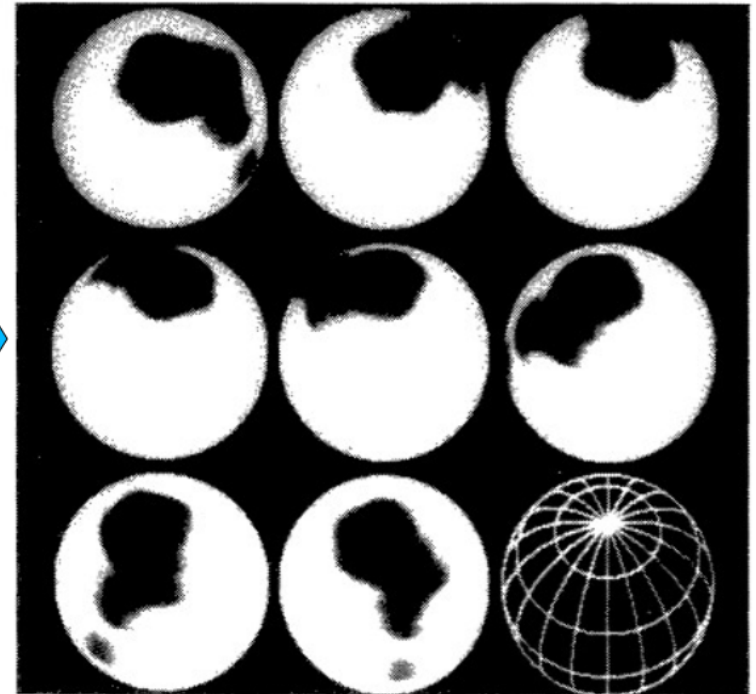
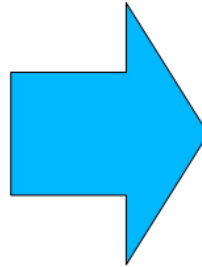
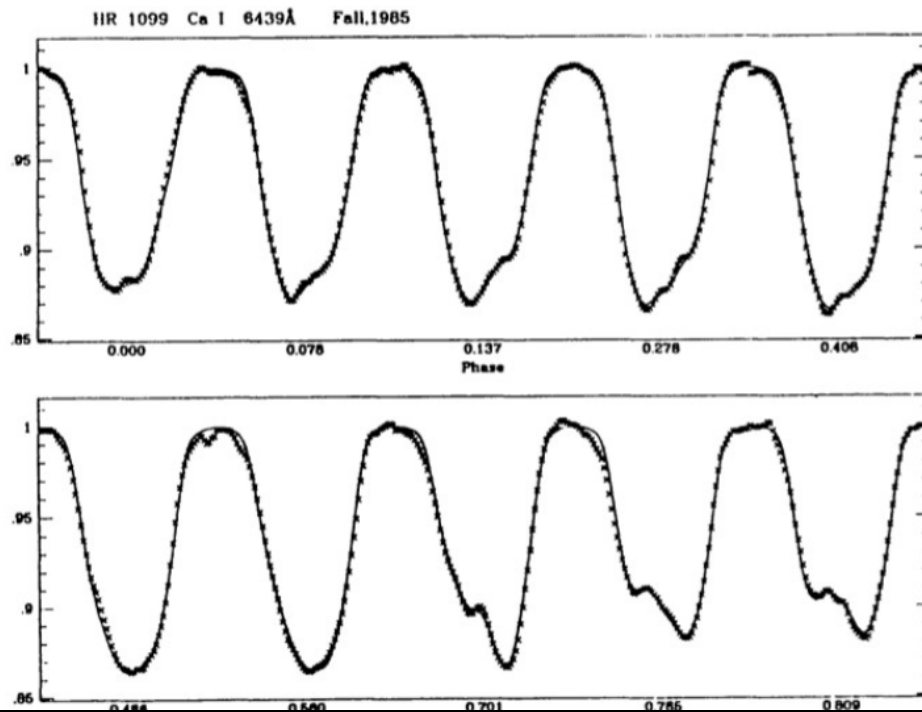
Extremely precise CO line lists in adequate models, a good statistics of lines, and the short distance of the brown dwarf allowed the determination of the surface features with high precision

# Comparing models from different authors

Estimated Teffs of brown dwarfs by Vrba et al. '04 & Golimowski et al. '04



# "Doppler Imaging" inverts varying line profiles into a global 2D map

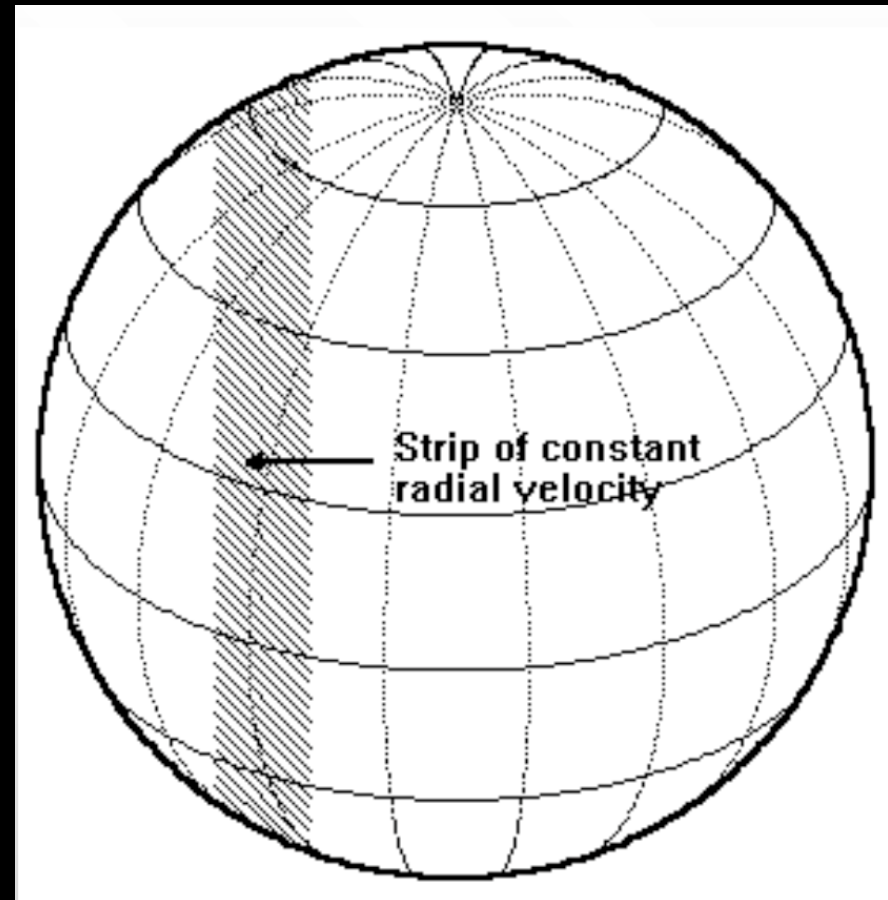


Vogt 1987

# Restrictions and efficiency

Nikolai Piskunov 2014

- The longitudinal resolution is usually determined by the PSF versus  $v \sin i$ . E.g. for  $v \sin i = 50$  km/s and the PSF = 5 km/s we may hope to resolve 40 elements along the stellar equator.
- In order to have a reliable reconstruction we should observe all the elements in many different combinations and Doppler shifts. In practice, sensible maps can be constructed already with 10 phases.

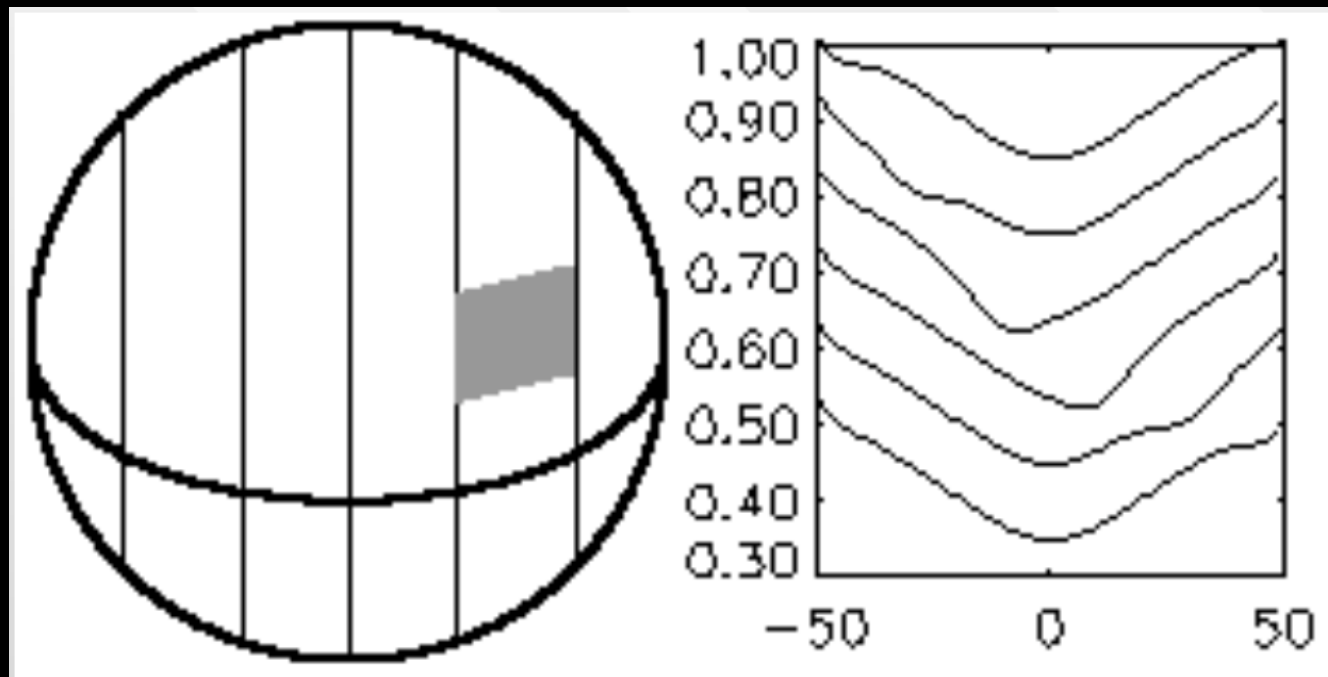




# Restrictions and efficiency

Nikolai Piskunov 2014

- The size of the surface element (in longitude) should not be larger than the width of a strip with "constant" (unresolved) radial velocity.
- The S/N ratio must be sufficient to identify the presence of a spot of a given contrast:



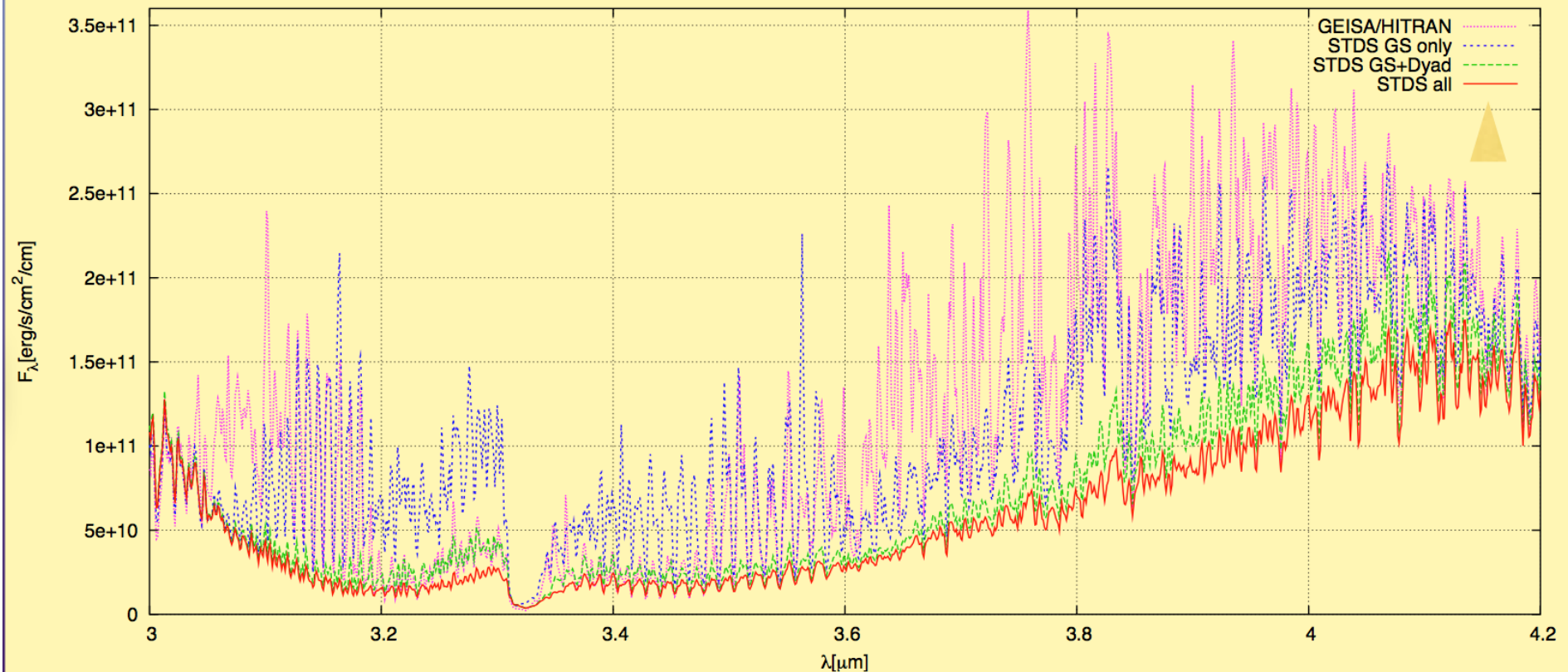
# Restrictions and efficiency

Nikolai Piskunov 2014

- An area near South Pole is not visible at any phase.
- Surface elements above the equator are visible more than half of the rotation.
- The elements near North Pole have small Doppler shifts.
- The best reconstruction must be expected in the belt of intermediate latitudes shifted North of equator by the inclination angle.
- For **pole-on and equator-on stars** the latitude information is lost.
- **Multiple chemical elements**. More than one element requires on the fly radiative transfer and multiple regularising functionals.
- DI of **active regions on late-type stars**. The temperature variation influences both line intensity and continuum, therefore different spectral lines can behave differently with temperature.
- **Eclipsing binaries**. The geometry becomes more complicated due to eclipses. Such systems have usually inclinations close to 90 degrees but the eclipse helps to break the symmetry.
- **Contact binaries**: non-spherical shape, variable surface gravity.
- Stars with accretion disks: warps, variable accretion, stellar spots due to accretion (bright) and magnetic activity (cool).

# Molecular Blanketing: $\text{CH}_4$

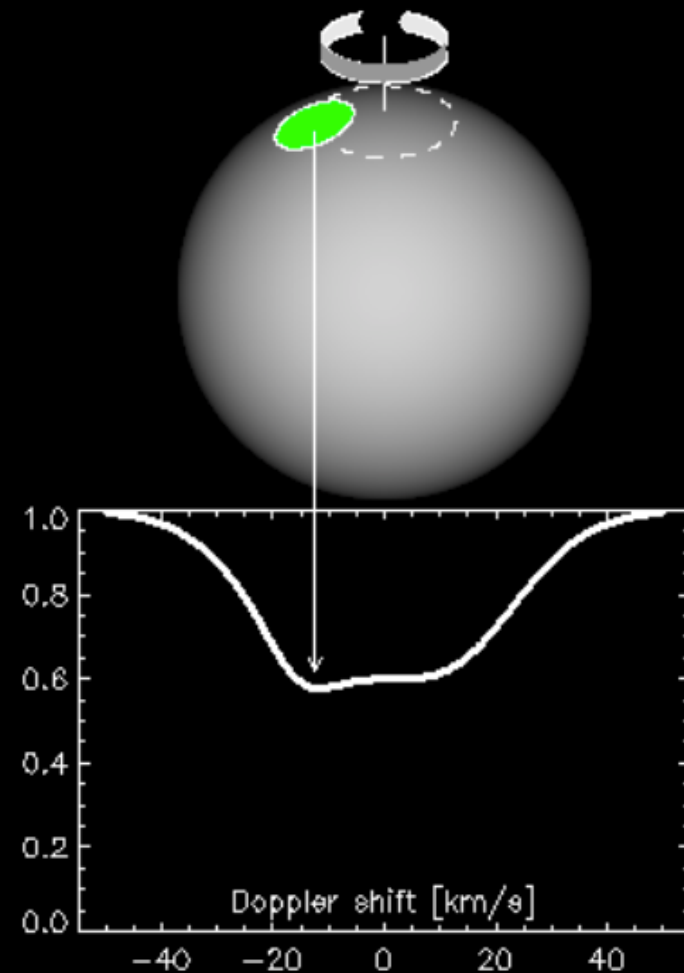
- 30 Mio. Lines computed with the STDS program (U. Bourgoigne - 2013 update: 80 Mio)
- Vibrational and rotational states up to  $\sim 8000 \text{ cm}^{-1}$
- Completeness :  $\sim 50\%$  (mid-IR) -  $10\%$  (H band) -  $0\%$  (Y/J band)



# Assumptions

Nikolai Piskunov 2014

- Each observed spectrum is taken during the time much shorter than the rotation period.
- The surface structures do not change throughout the observing run.
- The rotational broadening is larger than the instrumental profile (profiles are resolved).
- The star rotates as a solid body (no differential rotation).
- Chemical inhomogeneities do not affect the continuum.
- The wavelength scale of observations corresponds to the stellar reference frame.





# Phase Shifts of simultaneous HST light curves in different bands: the case of Luhman 16AB

*Biller et al. (2013)*

L7.5 + T0.5 @ 2 pc

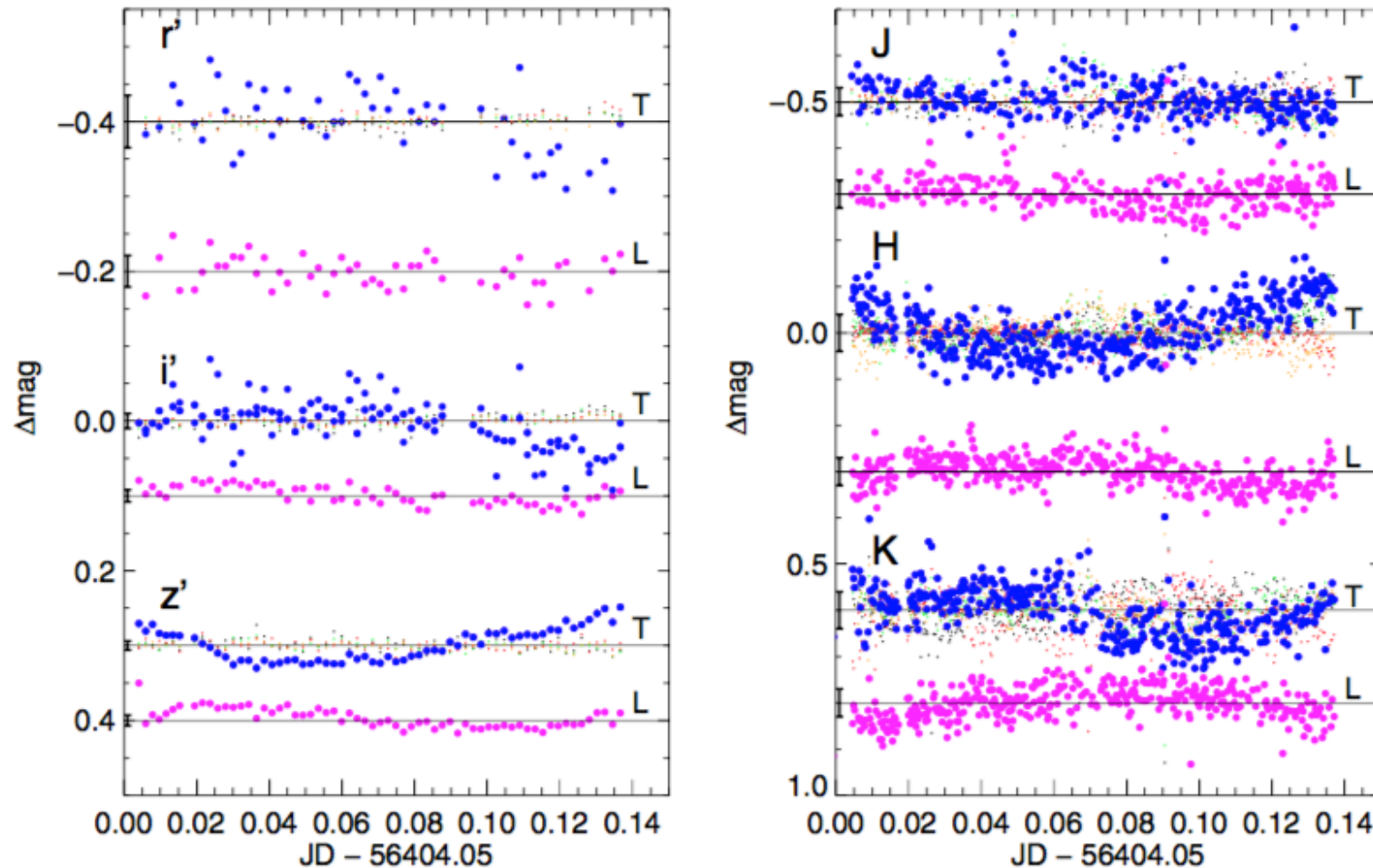
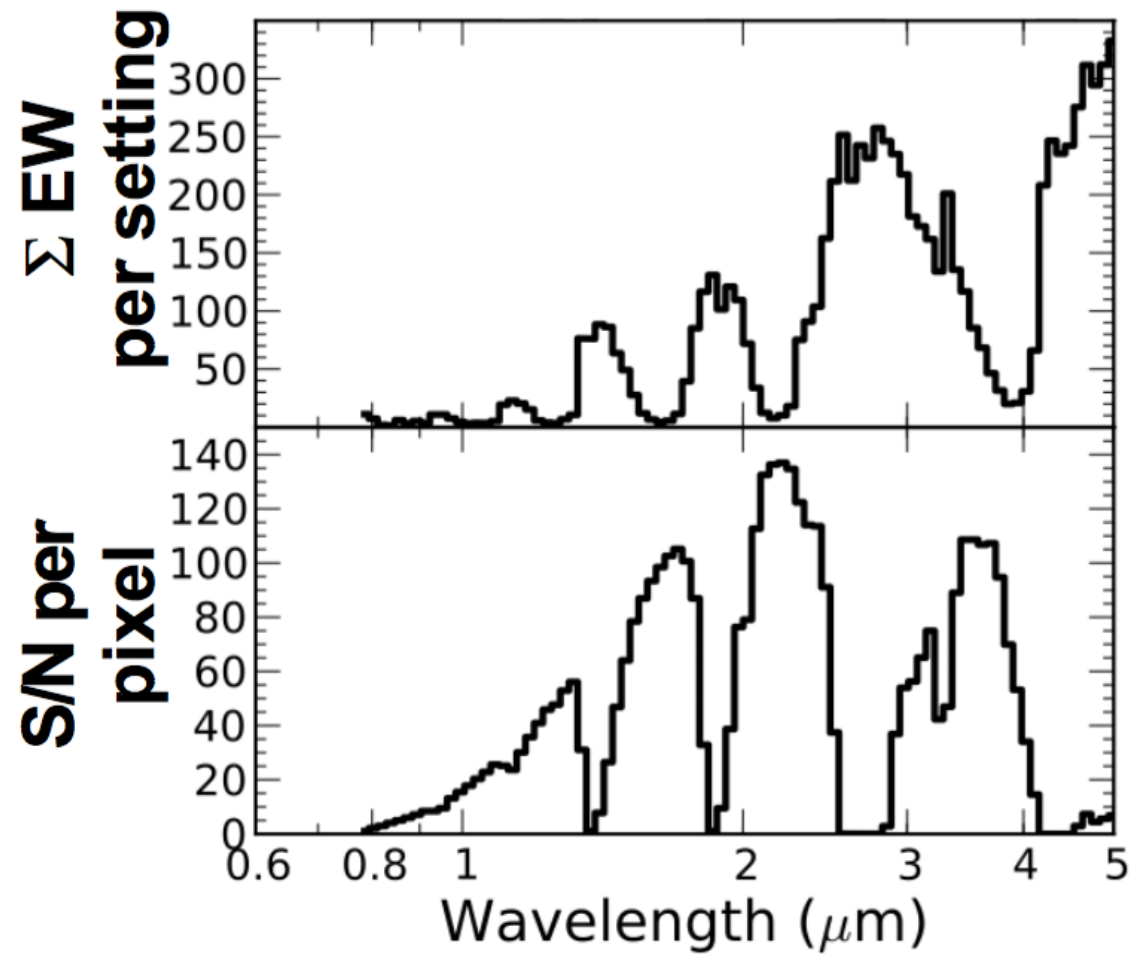
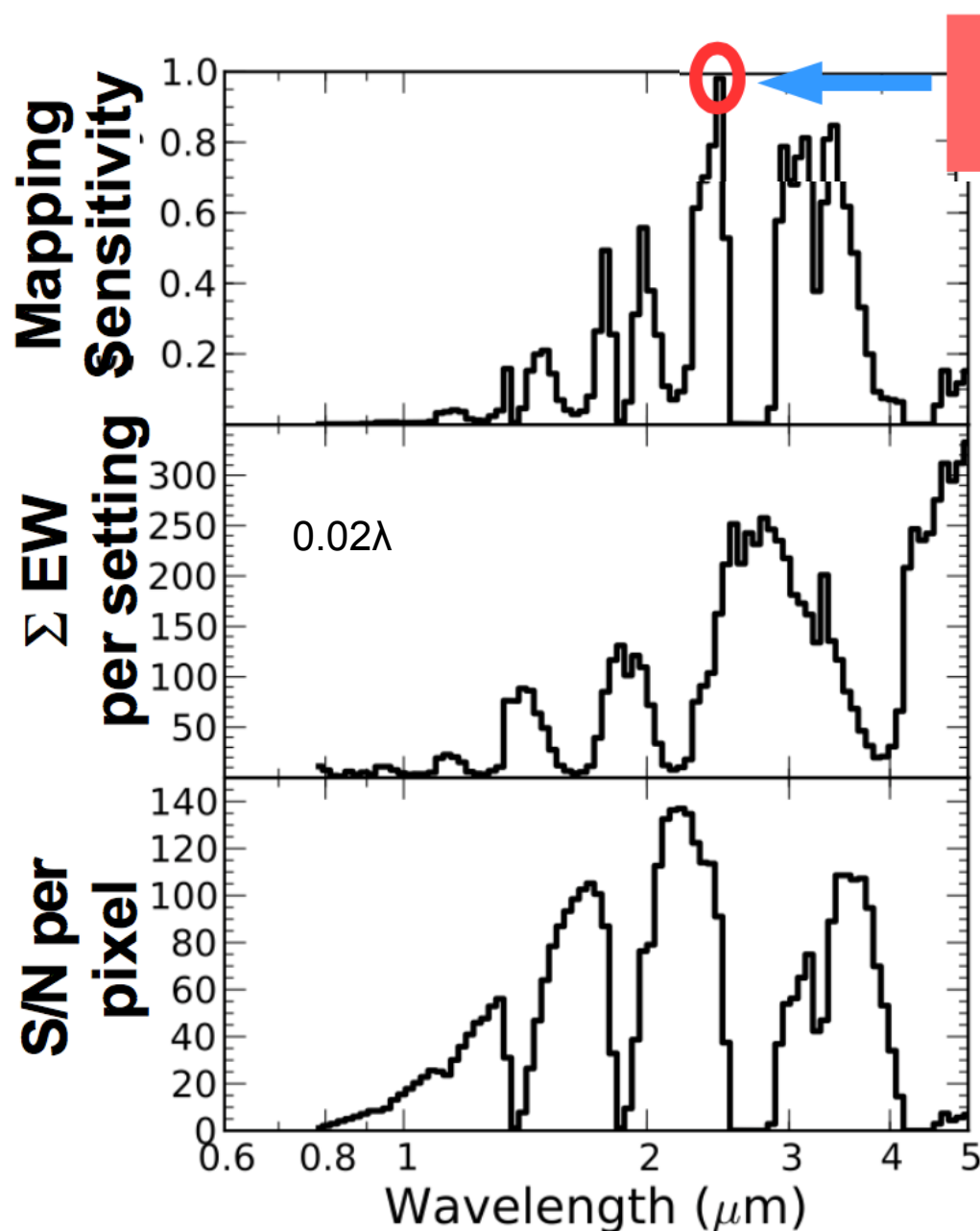


**Figure 3.** Single component light curves from PSF-fitting photometry on 2013 April 22 (UT). Estimated error bars are plotted at the beginning of each light curve and example residual reference light curves (reference star – high S/N reference light curve) are plotted as small dots.

Compute total Equivalent Width  
per  $0.02\text{\AA}$



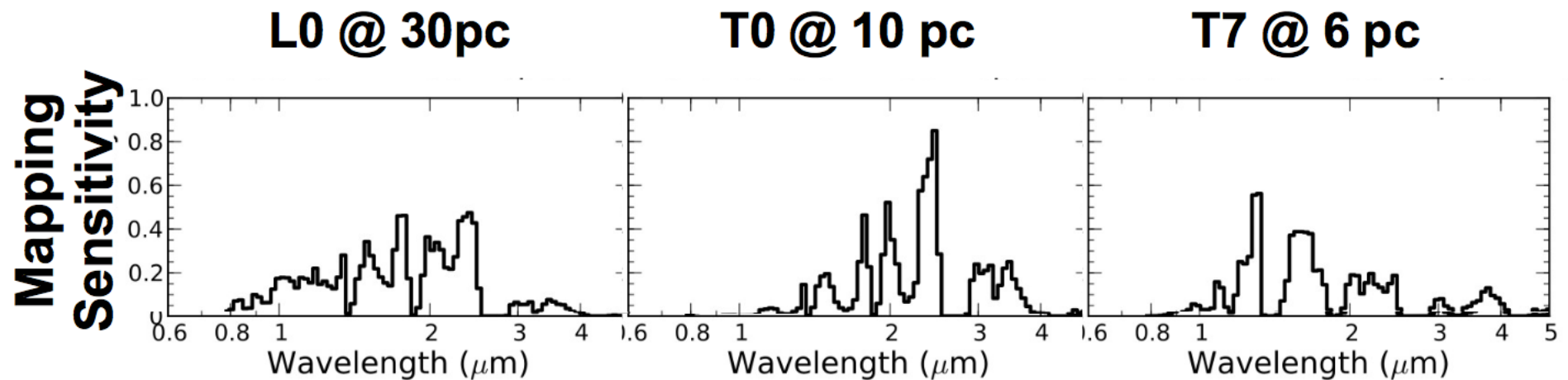
# Can we map other brown dwarfs?



Our CRIRES map comes from a single bin @ 2.3  $\mu\text{m}$ .

Sensitivity  $\sim$   
 $(\Sigma \text{ EW}) \times$   
 $(\text{S/N}) \times$   
(variability)

With E-ELT/ HIRES, dwarfs down to  $H \sim 13$  could be mapped using entire NIR spectrum

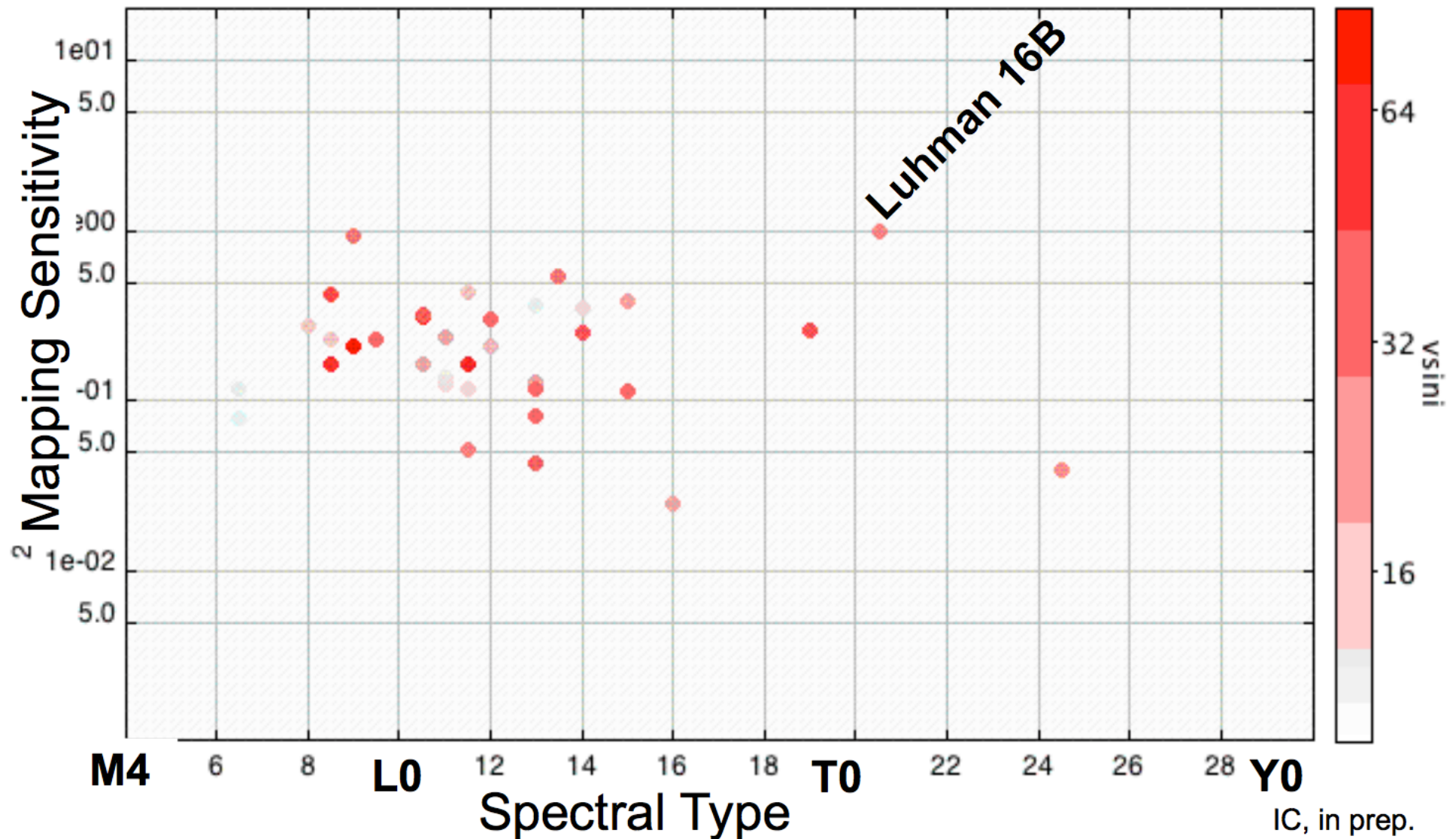


> 150 Brown Dwarfs !

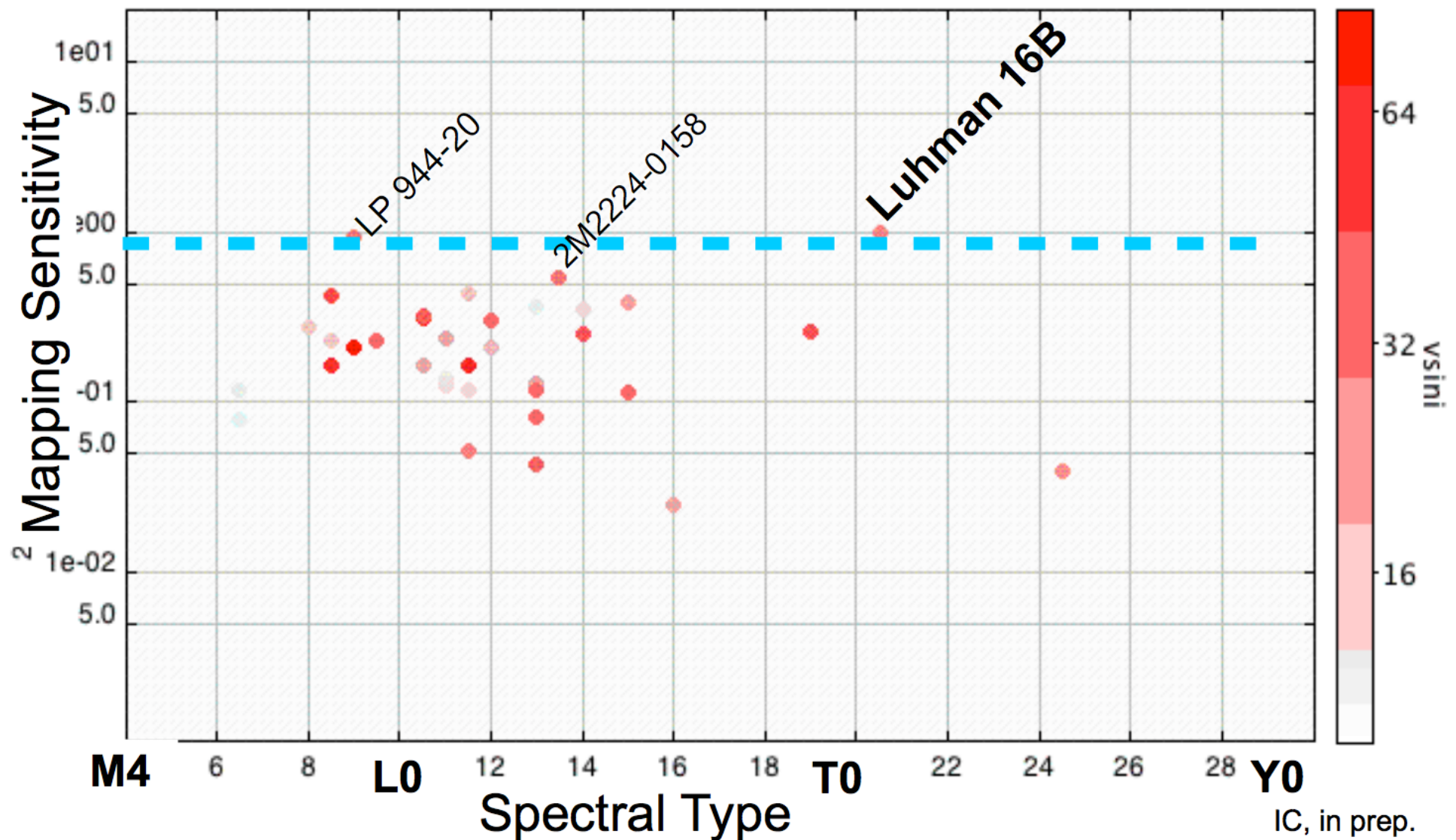
IC, in prep.



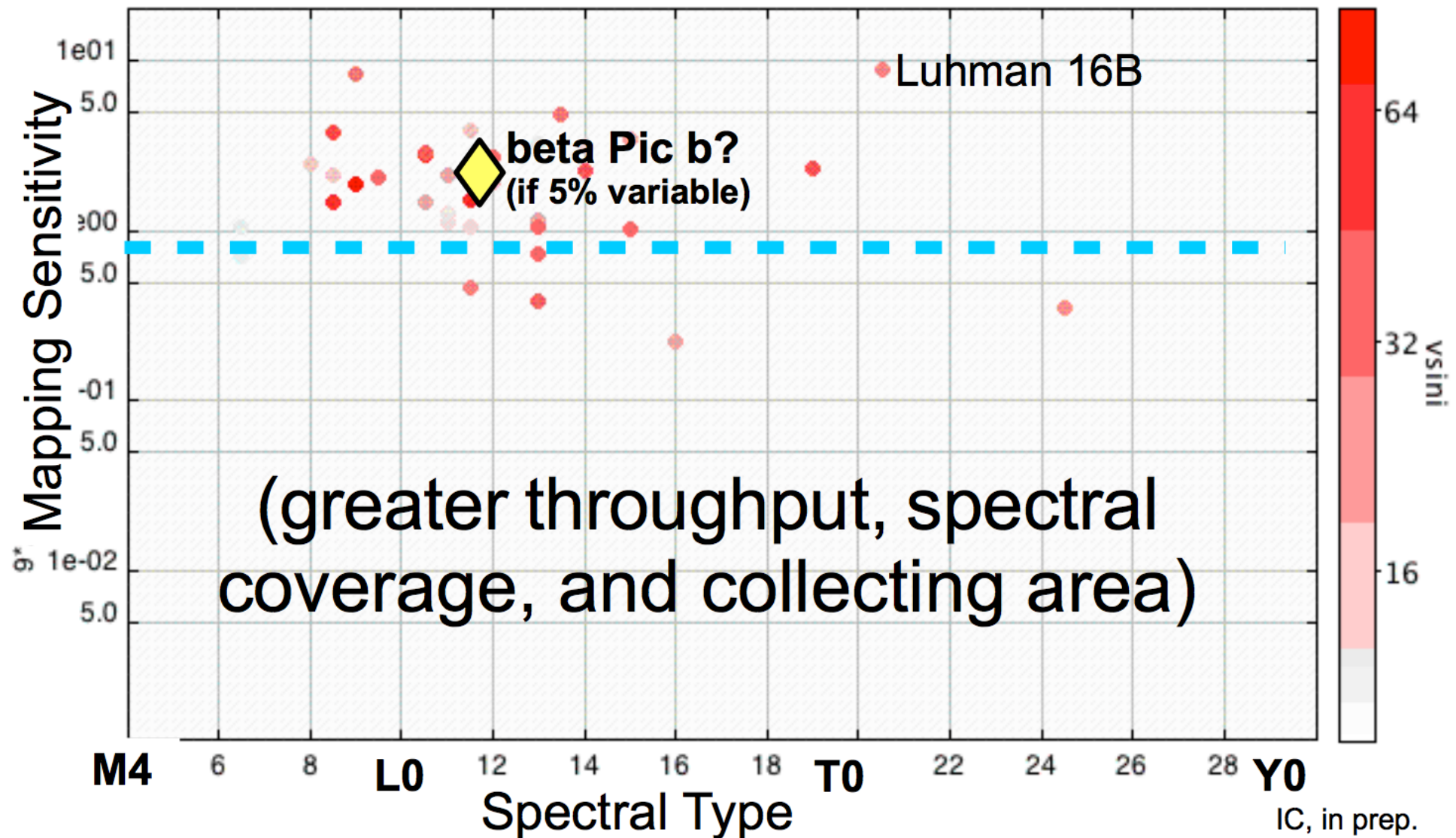
# Estimated "mapping sensitivity" for known variable brown dwarfs



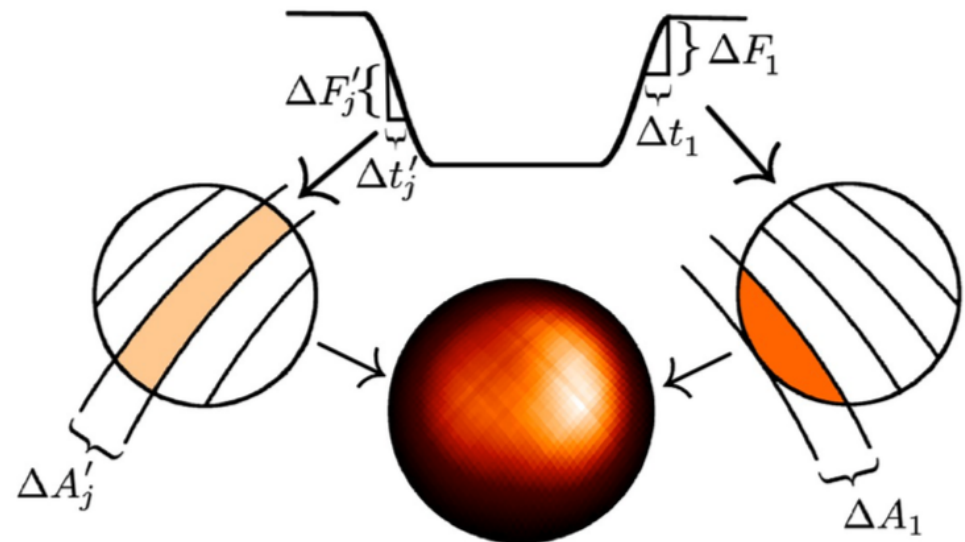
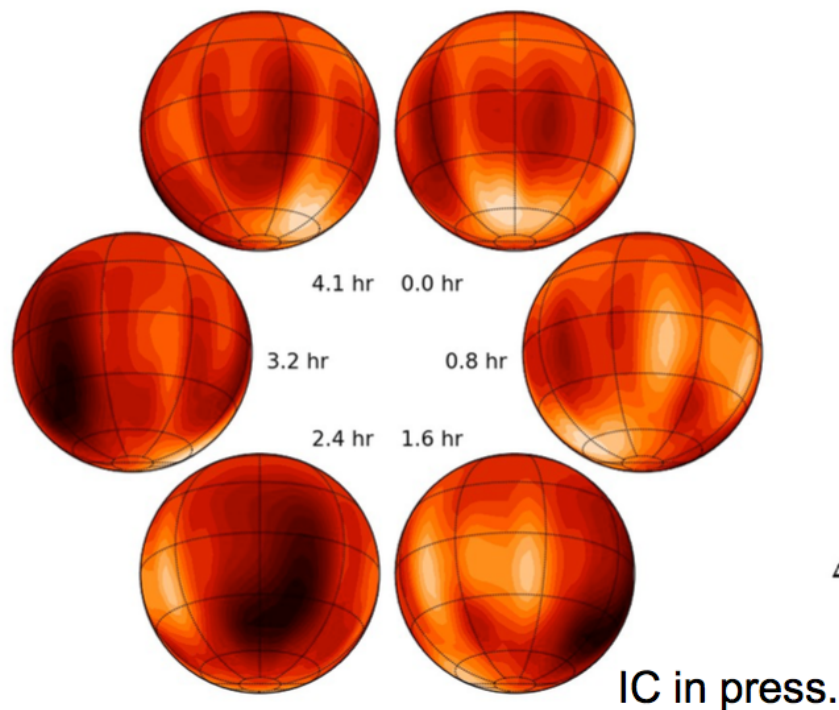
# Current CRIRES can map ~a few brown dwarfs



# E-ELT HIRES may even allow global mapping of giant exoplanets



# Doppler imaging is complementary to JWST exoplanet Science



Majeau+2012,  
de Wit+2012

Doppler Imaging of  
Planets & Brown Dwarfs  
with E-ELT

Eclipse mapping of giant,  
transiting exoplanets w/JWST



# Temperature fluctuations driven by deep atmospheric instabilities

Zhang & Showman (2014, *ApJ*, 788, L6)

The authors used a shallow-water model to investigate the global atmospheric dynamics in the stratified layer overlying the convective zone on these rapidly rotating objects.

The equations are derived from depth-integrating the Navier-Stokes equations, in the case where the horizontal length scale is much greater than the vertical length scale. Under this condition, conservation of mass implies that the vertical velocity of the fluid is small. It can be shown from the momentum equation that vertical pressure gradients are nearly hydrostatic, and that horizontal pressure gradients are due to the displacement of the pressure surface, implying that the horizontal velocity field is constant throughout the depth of the fluid. Vertically integrating allows the vertical velocity to be removed from the equations. The shallow water equations are thus derived.

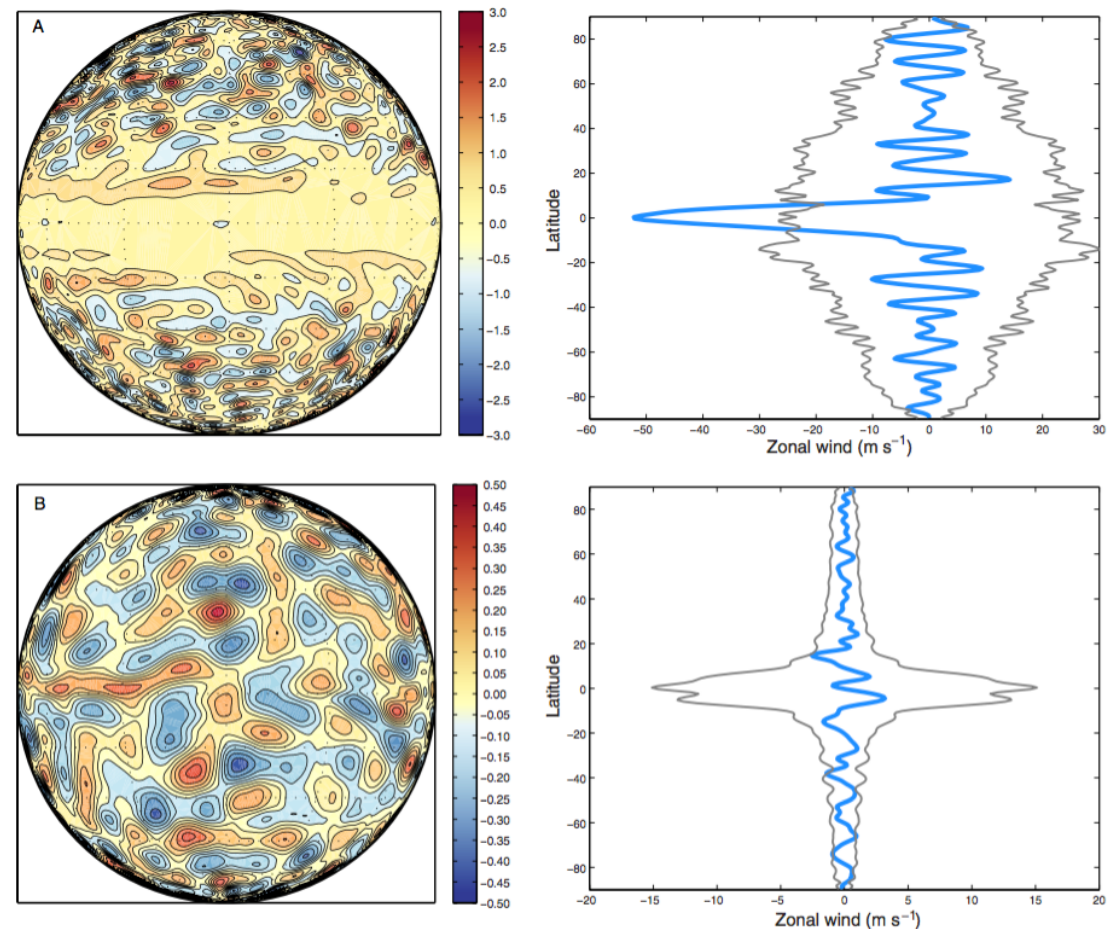


Figure 1. Two atmospheric regimes of brown dwarfs ( $\Omega \sim 10^{-3} \text{ s}^{-1}$ ) under forcing wavenumber 40. Upper panel: jet case (case A); lower panel: isotropic turbulence case (case B). Left panel: geopotential anomaly map (in units of  $10^5 \text{ m}^2 \text{ s}^{-2}$ ); right: zonal-mean zonal wind (blue) and standard deviation in longitude of the zonal wind at each latitude (gray). Both models have a small deformation radius of  $\sim 10^3 \text{ km}$ .

# Temperature fluctuations driven by deep atmospheric instabilities

Zhang & Showman (2014, ApJ, 788, L6)

The authors used a shallow-water model to investigate the global atmospheric dynamics in the stratified layer overlying the convective zone on these rapidly rotating objects.

They found that jets or eddy circulation in stratified layers, is important in late-T dwarfs, which radiative time scale is long enough to support temperature fluctuations dissipation on longer time scales than a minute.

The radiative relaxation timescale ( $\tau_{\text{rad}}$ ) is estimated to be :

$$\tau_{\text{rad}} \sim P c_p / g 4\sigma T^3$$

Where  $P$  is the pressure of the typical photosphere level ( $\tau \sim 1$ ). For a typical brown dwarf of  $\sim 1000\text{K}$ , the radiative timescale is  $\sim 10^5\text{s}$ . Since the  $T_{\text{eff}}$  of brown dwarfs ranges from several hundred (e.g., Y type) to several thousand kelvins (e.g., L0 type), the radiative timescale can vary by several orders of magnitude ( $\sim 10^4$ - $10^7$  s). By comparison, the radiative relaxation timescale for Jupiter is  $\sim 10^9\text{s}$ . Radiative cooling might also be important for cloud formation on brown dwarfs (Helling et al. 2001).

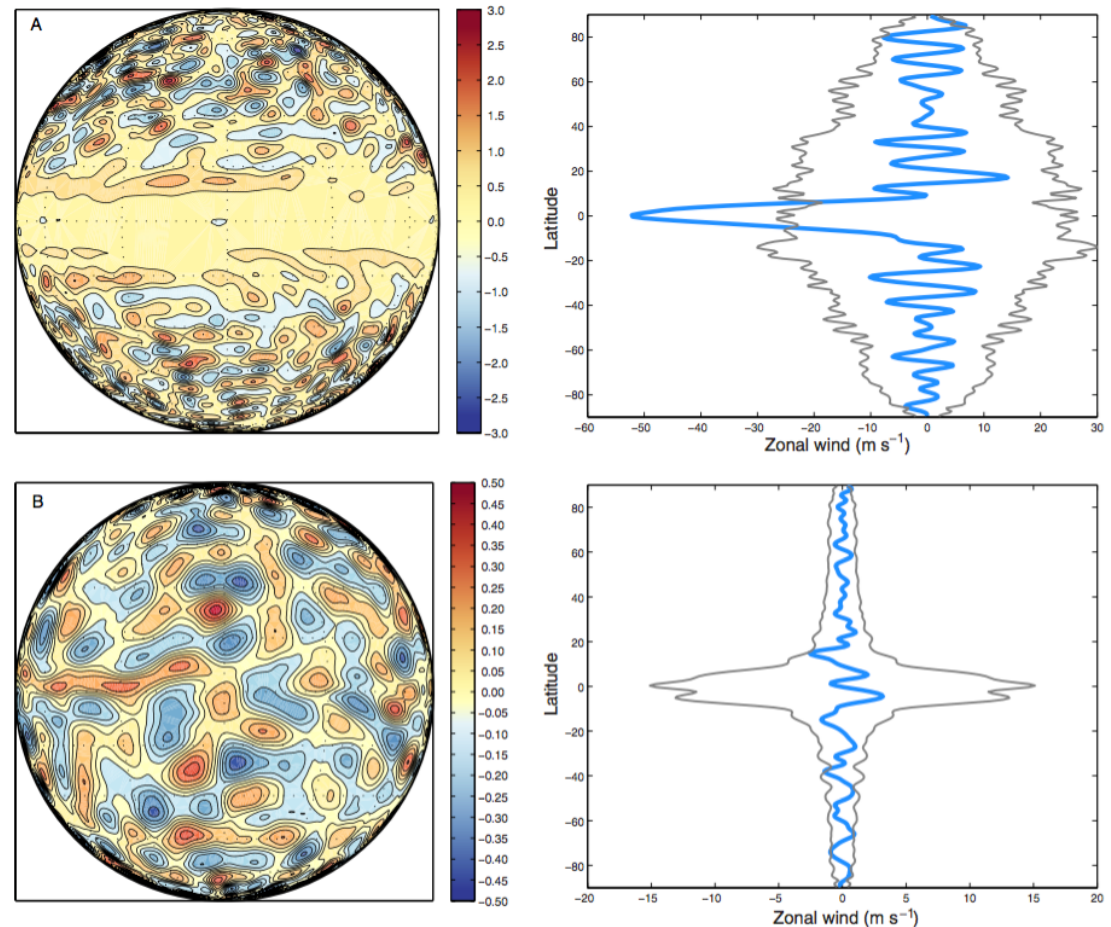


Figure 1. Two atmospheric regimes of brown dwarfs ( $\Omega \sim 10^{-3}\text{s}^{-1}$ ) under forcing wavenumber 40. Upper panel: jet case (case A); lower panel: isotropic turbulence case (case B). Left panel: geopotential anomaly map (in units of  $10^5 \text{ m}^2 \text{ s}^{-2}$ ); right: zonal-mean zonal wind (blue) and standard deviation in longitude of the zonal wind at each latitude (gray). Both models have a small deformation radius of  $\sim 10^3$  km.

# Brown Dwarfs Ionized ?

Radio and X-ray observations and theoretical studies suggest brown dwarf atmospheres to be ionized. Helling et al. (2011a,b) have shown that clouds in brown dwarfs are charged, and that clouds can discharge in form of lighting (Bailey et al. 2013). **Cosmic Rays** can ionize the upper atmosphere and the upper part of the cloud (Rimmer & Helling 2013). And **hydrodynamic winds** can provide a source for gas-ionization (Stark et al. 2013). This figure shows that these ionization processes (boxes) do appear with different efficiencies in different parts of the atmosphere, suggesting a brown dwarf atmosphere to be a **stratified ionized medium** rather than a cold, neutral gas.

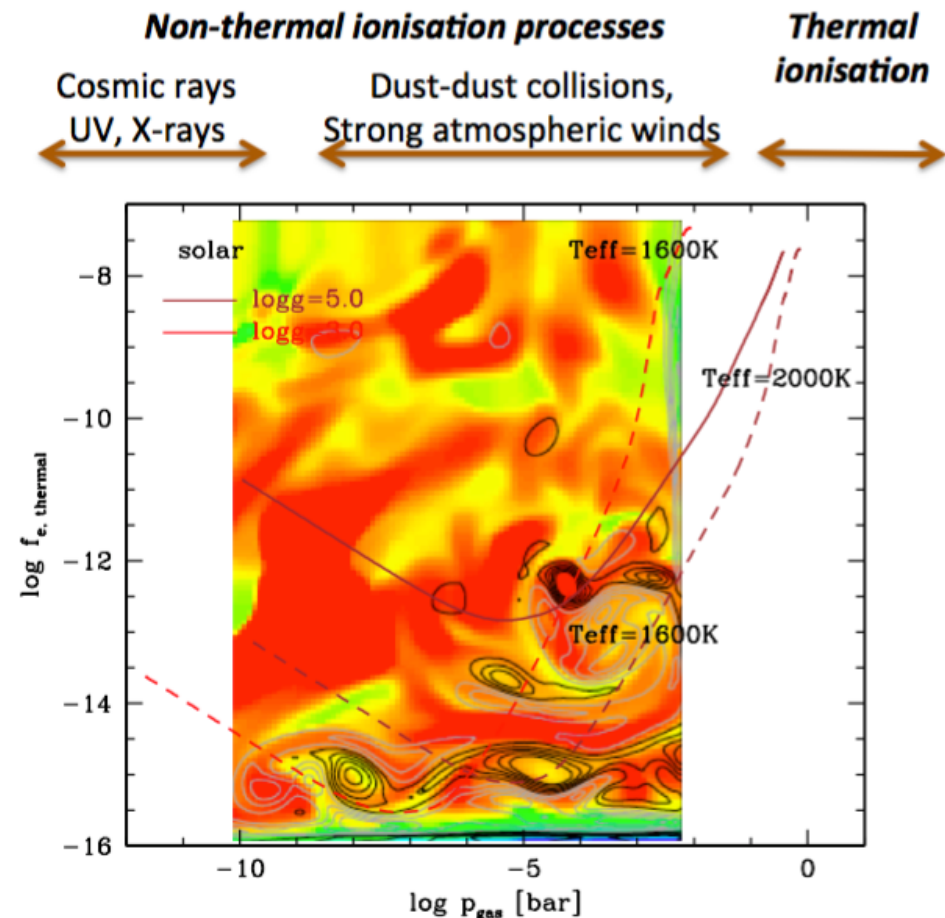
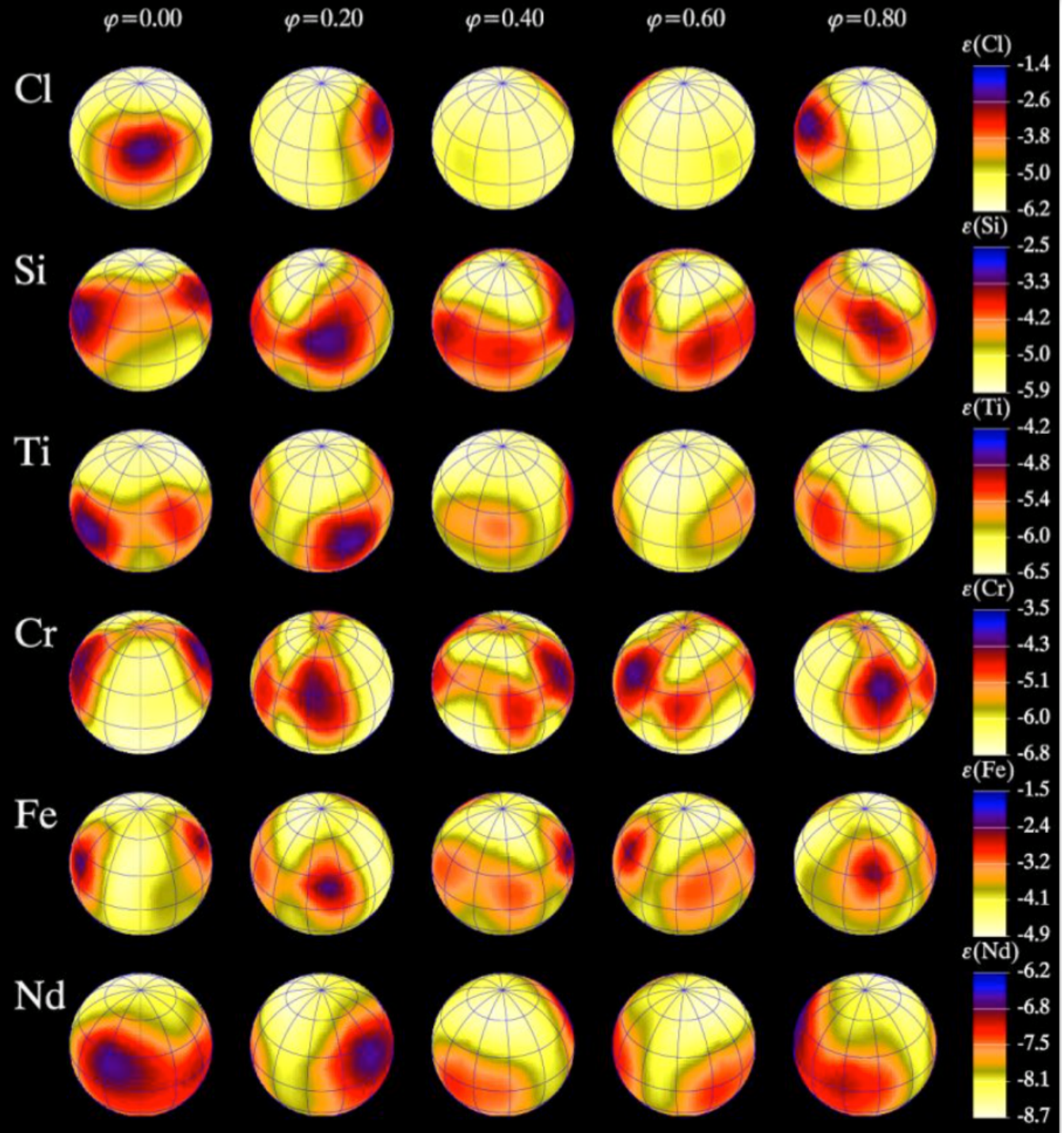


Fig. 13 A brown dwarf atmosphere is not only stratified by its cloud structure (2D colour overlay). Different non-thermal ionization processes occur in brown dwarf atmospheres (boxes: cosmic rays, dust-dust collisions, strong winds) which produce free charges through the atmosphere with varying efficiency. The local degree of thermal ionization (brown solid and dashed lines) is shown in the background for illustration, a 2D simulation of turbulent dust formation indicates where the cloud is located in the atmosphere. (The 2D colour-coded plot contains contour lines of the local vorticity; see Fig 8 in [Helling et al \(2004\)](#))



# Chemically Peculiar Stars

The atmospheres of slowly rotating main sequence A and B stars are very stable, and this in turn allows several remarkable processes to operate. The most prominent characteristic of many CP stars is the presence of **strong fossil magnetic fields** at their surfaces and in interiors. Moreover, due to the atmospheric stability, further enhanced by the magnetic field, **chemical segregation processes**, determined by the competition between **gravitational settling** and **radiative levitation**, can operate efficiently.

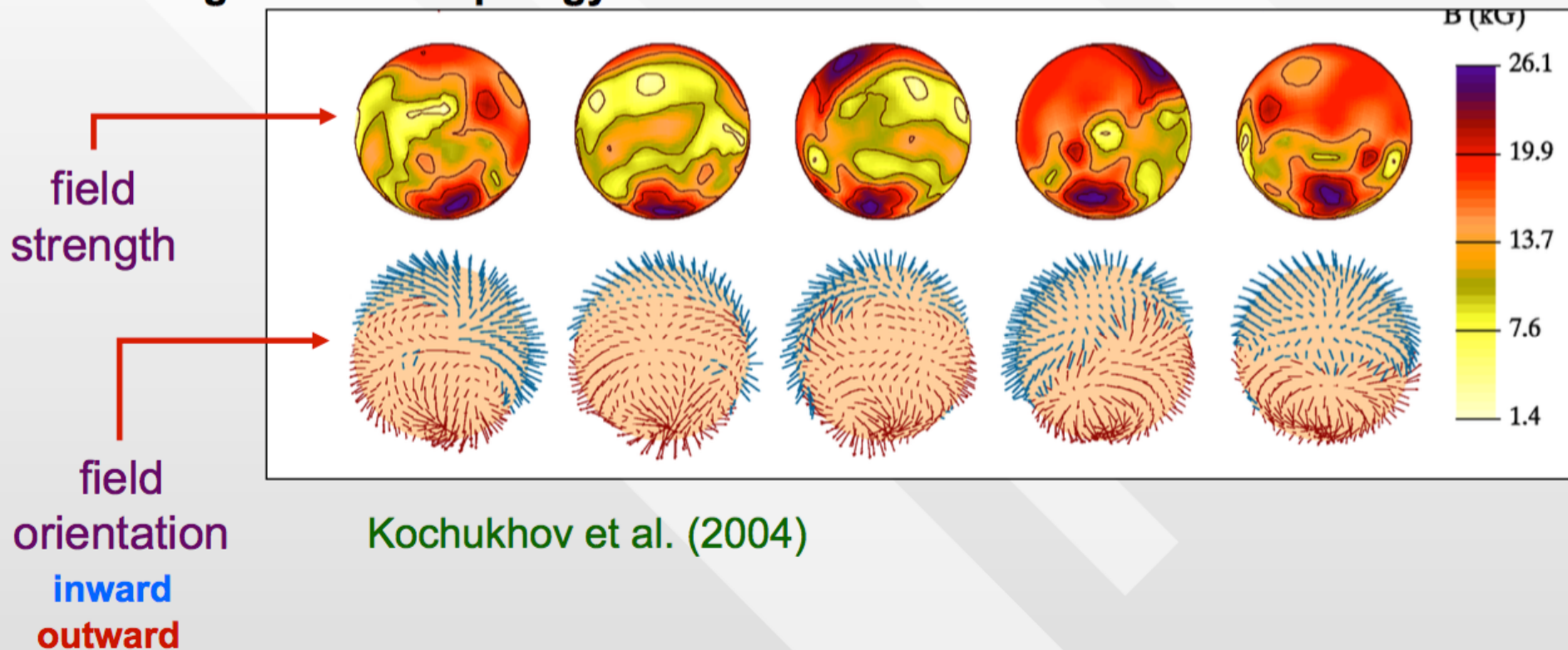




# Chemically Peculiar Star

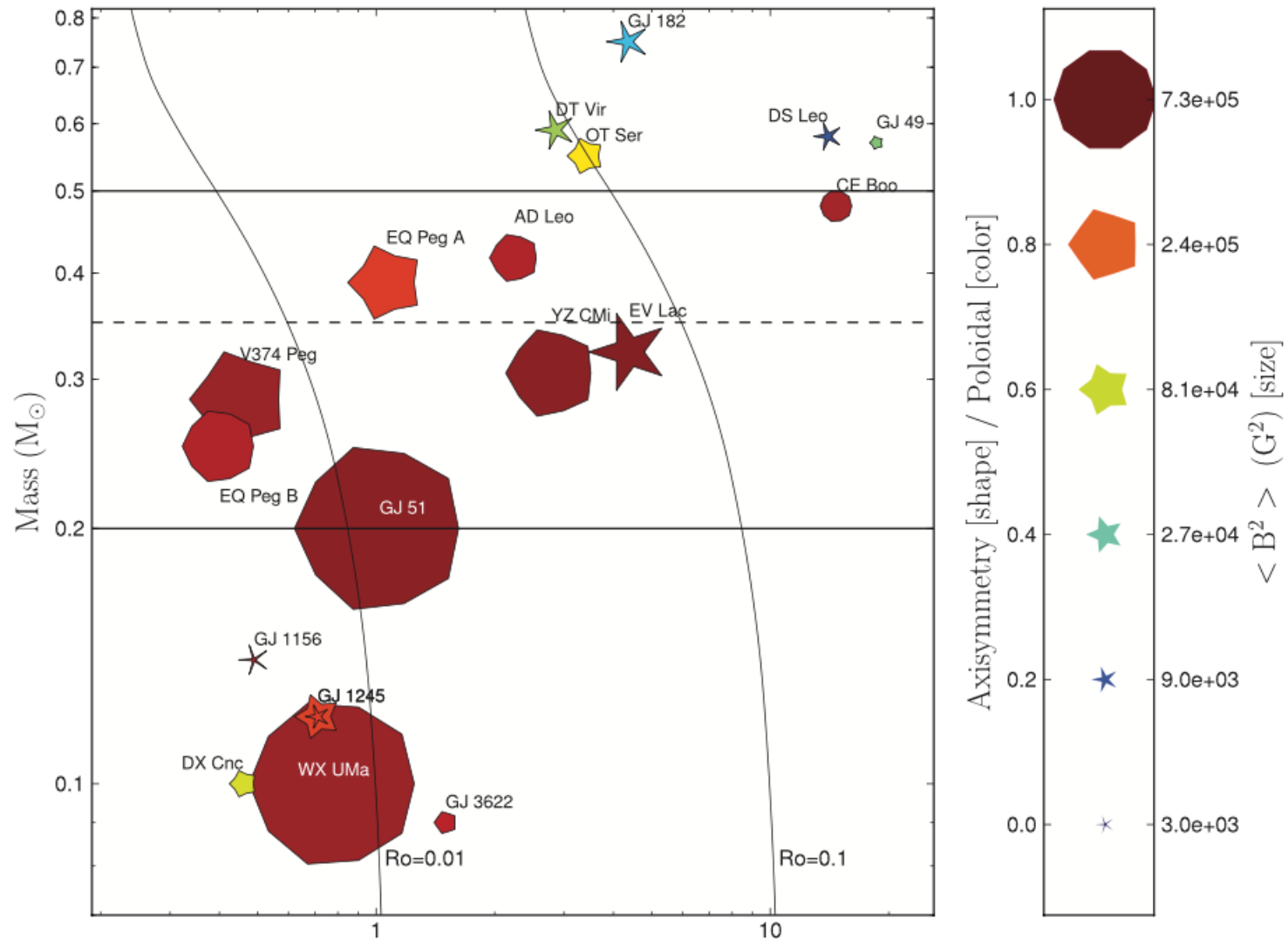
## Magnetic Doppler Imaging

Magnetic field topology of 53 Cam inferred with MDI




Kochukhov et al. (2004)

**M Dwarf  
Magnetic  
field  
measured  
from the  
spectral  
analysis of  
spectral line  
in  
polarimetry  
and Zeeman  
splitting**



*Morin et al.  
2010, 2011*

The average value of the scalar magnetic field at the surface of the star is inferred from the analysis of the **Zeeman broadening of spectral lines** (Saar 1988, Reiners & Basri 2006). **Time-series of circularly polarized spectra** and tomographic imaging techniques to produce spatially resolved maps of the large-scale component (typically up to spherical harmonic degree  $l_{\max}$  in the range 6-30, depending on the rotational velocity) of the vector magnetic field (**Zeeman-Doppler Imaging**, Semel 1989, Donati & Brown 1997, Donati et al. 2006b).

- 
- E-ELT HIRES & METIS can map dozens of brown dwarfs, and a few bright exoplanets
  - This work will produce global maps and weather movies of brown dwarf atmospheric chemistry, dynamics, and cloud properties

## What do we need?

- High spectral resolution ( $R > 50,000$ )
- Broad, *simultaneous* spectral coverage
- High efficiency (AO w/infrared WFS would help)
- More measurements (w/higher precision) of brown dwarf variability, rotation periods, and  $v \sin i$

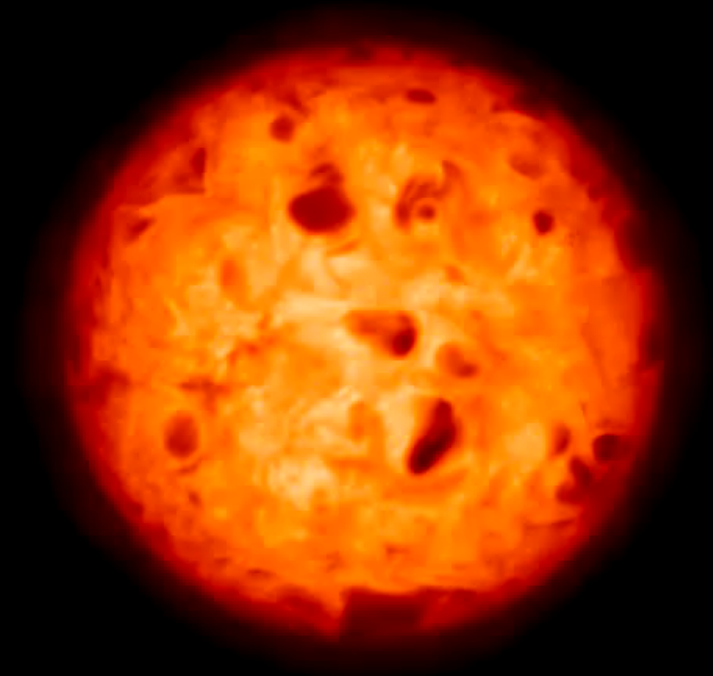
# Scaled Global simulations

*Freytag & Allard 2015 (in prep.)*

st22g35n07: Surface Intensity(21), time( 1.0)=350503.0 s

CO5BOLD "Star in the box" RHD simulation with a radius 20 times smaller than the true radius.

Here the spatial resolution is not enough to resolve the small-scale gravity waves, and not enough momentum is released to generate the laminar flow. Only overshoot is responsible for the formation of clouds in this simulation.



*T<sub>eff</sub>= 2200K, logg= 3.5, solar*



## Scaled Global simulations

*Freytag & Allard 2015 (in prep.)*

CO5BOLD "Star in  
simulation with a  
smaller than the t

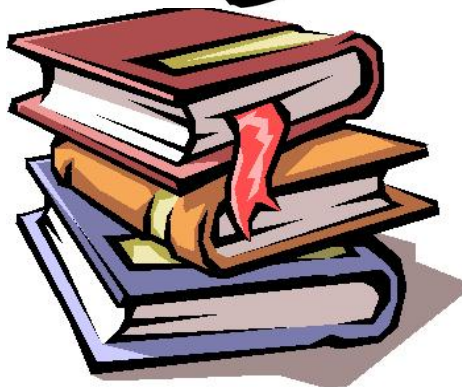
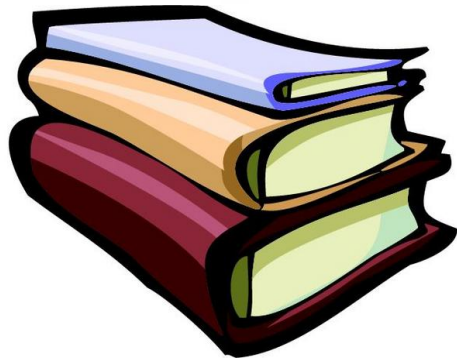
Here the spatial resolution is not enough to resolve gravity waves, and not enough momentum is released to generate the laminar flow. Only overshoot is responsible for the formation of clouds in this simulation.

RHD simulations of cloud formation are currently in their infancy, but by the time of the E-ELT first light in 2024 RHD and MHD simulations with 3D radiative transfer will be available also on multi-node machines to further the knowledge on these atmospheres!

$T_{\text{eff}} = 2200\text{K}$ ,  $\log g = 3.5$ , solar

# Main original actors of exoplanet field

authors	geometry	opacities	chemistry	radiative transfer
Barman et al. '01, '05, '06 Barman '08	1D, hydrostatic Global 3D reconstruction	Gas + dust	CE, NLTE, Photo-ionization	Spherical symmetry, ALI
Sudarsky et al. '03,'05,'06 Burrows et al.'03,'04,'05,'06	1D, hydrostatic	Gas + dust	CE	Plan-parallel, ALI
Seager et al. '98, '00, '05	1D, hydrostatic	Gas + dust	CE	Plan-parallel (Feautrier)
Fortney et al. '05, '06	1D, hydrostatic	Gas + dust	CE by table interpolation	Plan-parallel, two-stream, NO scattering
Brown '01, Tinetti et al. '08	Ray tracing, hydrostatic Ad-hoc rotation	Gas + dust	CE, Photo-ionization Photochemistry	
Goukenleuque et al. '00, Iro et al. '05	1D, time relaxation, Ad-hoc rotation, Global 3D reconstruction	Gas + dust	CE not updated with time	Plan-parallel, two-stream, WITH scattering
Freytag et al. '10, '15	Local & global 3D Hydrodynamics, winds, rotation	Gas + dust	CE	3D (Feautrier)
Showman & Guillot '02	Local 3D hydrodynamics, winds	-	-	Radiative gradient from RT models
Dobbs-Dixon & Lin '07	Global 3D hydrodynamics, rotation	Dust only	CE	Diffusion approximation
Cho et al. '96, '01, '03, '07 Menou '03	Global 2D (single layered) hydrodynamics, rotation	-	-	-



# Some reading

- Helling & Casewell, “*Atmospheres of Brown Dwarfs*”, *A&A Review*, Vol. 22, article id.80, pp.45, 2014
- Seager & Deaming, “*Exoplanet Atmospheres*”, *Annual Review of A&A*, Vol. 48, p. 631-672, 2010
- Chabrier & Baraffe, “*Theory of low-mass stars and substellar objects*”, *Annual Review of A&A*, Vol. 38, p. 337-377, 2000
- Norlund, Stein & Asplund, “*Solar Surface Convection*”, *Living Reviews of Stellar Physics*, 2009 (online)
- Bohren & Huffman, “*Absorption and scattering of light by small particles*”, *Wiley Science Paperback Series*